

Semi-analytic modelling of galaxy evolution in the IR/submm range

Bruno Guiderdoni,¹ Eric Hivon,² François R. Bouchet,¹ and Bruno Maffei³

¹ *Institut d’Astrophysique de Paris, CNRS, 98bis Boulevard Arago F–75014 Paris France*

² *Theoretical Astrophysics Center, Juliane Maries Vej 30, DK–2100 Copenhagen Denmark*

³ *Queen Mary and Westfield College, Mile End Road, London E1 4NS UK*

2 December 2024

ABSTRACT

This paper proposes a new semi-analytic modelling of galaxy properties in the IR/submm wavelength range, which is explicitly set in a cosmological framework. We start from a description of the non-dissipative and dissipative collapses of primordial perturbations, and add star formation, stellar evolution and feedback, as well as the absorption of starlight by dust and its re-emission in the IR and submm. This type of approach has had some success in reproducing the *optical* properties of galaxies. We hereafter propose a simple extension to the IR/submm range. The growth of structures is followed according to the standard Cold Dark Matter model. We assume that star formation proceeds either in a “quiescent” mode, e.g. as in disks, or in a “burst” mode with ten times shorter time scales. In order to reproduce the current data on the evolution of the comoving cosmic SFR and gas densities, we need to introduce a mass fraction involved in the “burst” mode strongly increasing with redshift, probably reflecting the increase of interaction and merging activity. We estimate the IR/submm luminosities of these “mild starburst” and “luminous UV/IR galaxies”, and we explore how much star formation could be hidden in heavily-extinguished, “ultraluminous IR galaxies” by designing a family of evolutionary scenarios which are consistent with the current status of the “cosmic constraints”, as well as with the *IRAS* 60 μm luminosity function and faint counts, but with different high- z IR luminosity densities. However, these scenarios generate a Cosmic Infrared Background whose spectrum falls within the $\pm 1\sigma$ range of the isotropic IR component detected by Puget *et al.* (1996) and revisited by Guiderdoni *et al.* (1997). We give predictions for the faint galaxy counts and redshift distributions at IR and submm wavelengths. The submm range is very sensitive to the details of the evolutionary scenarios. As a result, the on-going and forthcoming observations with *ISO* and SCUBA (and later with *SIRTF*, *SOFIA*, *FIRST* and *PLANCK*) will put strong constraints on the evolution of galaxies at $z \sim 1$ and beyond.

Key words: cosmology – galaxy formation – galaxy evolution – infrared – submm.

1 INTRODUCTION

This paper describes a new modelling of galaxy evolution in the infrared and submm wavelength ranges, which are now open to high-redshift exploration by the on-going observations with *ISO* and SCUBA, and forthcoming facilities and experiments such as *SIRTF*, *SOFIA*, *FIRST* and *PLANCK*.

As a matter of fact, our knowledge of the early epochs of galaxies has recently increased thanks to the richness and precision of the observational evidence obtained by UV/visible/NIR surveys of high-redshift objects (Lilly *et al.* 1995; Ellis *et al.* 1996; Cowie *et al.* 1996; Steidel *et al.* 1996; Williams *et al.* 1996). The pattern of galaxy evolution which

emerges from these data can be summarized as follows: i) Faint galaxy counts show the presence of a large number of blue objects, well in excess of no-evolution expectations (Williams *et al.* 1996). ii) These blue objects are “sub- L^* ” galaxies undergoing strong bursts of star formation (Lilly *et al.* 1996; Ellis *et al.* 1996). iii) The fraction of these blue objects with unclassified/peculiar morphologies showing signs of tidal interaction and merging (Abraham *et al.* 1996) increases from local samples to the HST high-resolution observations of the Medium Deep Survey (Griffiths *et al.* 1994) and Hubble Deep Field (Williams *et al.* 1996). iv) The global star formation rate (hereafter SFR) of the universe declined by a factor of about ten since redshift $z \sim 1$ (Lilly *et al.*

1996; Madau *et al.* 1996; Sawicki *et al.* 1997; Connolly *et al.* 1997). v) Finally, this high SFR seems to be correlated to the decrease of the cold-gas comoving density associated with damped Lyman- α systems between $z = 2$ and $z = 0$ (Storrie-Lombardi *et al.* 1996). These results nicely match a picture in which star formation in bursts triggered by interaction/merging consumes the gas content of galaxies as time goes on. It is common wisdom that such a qualitative scenario is expected within the paradigm of hierarchical growth of structures. The implementation of hierarchical galaxy formation in semi-analytic models quantitatively substantiates this view and may further suggest that we have seen the bulk of star formation and understood the broad features of galaxy formation (Baugh *et al.* 1997).

However, it should be emphasized that this seemingly consistent view is entirely based on visible/NIR observations which only probe the rest-frame UV/visible light of high- z objects. The total amount of energy released by star formation should be estimated by summing up the UV/visible/NIR light of stellar populations directly escaping from galaxies, *and* the part which has been absorbed by dust and re-emitted in the IR/submm wavelength range. The corrections needed to account for optical extinction by dust are rather uncertain and could easily induce an upward revision of the high-redshift SFR deduced from rest-frame UV/visible observations by factors of a few. Moreover, a significant fraction of star formation might be completely hidden in heavily-extinguished galaxies which are missed by the above-mentioned surveys. Even for normal objects like spiral galaxies, the fraction of energy emitted in the IR can amount to 30 % of the optical, and this can increase to more than 95 % for ultraluminous starbursts. As a matter of fact, the IR/submm range might be more adequate than the optical for observing high-redshift, starburst galaxies provided they are dusty. The rest-frame IR/submm spectrum of dust heated by a young stellar population peaks between 50 to 100 μm , pointing out the submm range as particularly relevant for the search of primeval, high-redshift galaxies.

At this time, we know very little about the “optically-dark” side of galaxy evolution. The *IRAS* satellite has given the first complete survey of FIR galaxy properties, in four bands between 12 and 100 μm . Many studies have emphasized the wide variety of IR luminosities, from “normal spirals” to “mild starbursts”, and finally to the “luminous IR galaxies” (hereafter LIGs), mostly interacting systems, and the spectacular “ultraluminous IR galaxies” (hereafter ULIGs), which are mergers (Sanders and Mirabel 1996; Clements *et al.* 1996b). Unfortunately, while we have learned from *IRAS* that about one third of the bolometric luminosity of the local universe is released in the IR/submm (Soifer and Neugebauer 1991), we know very little about galaxy evolution in this wavelength range. Faint galaxy counts and redshift surveys down to flux densities $S_\nu \sim 60$ mJy (at 60 μm) do not probe deeper than $z \sim 0.2$ (Ashby *et al.* 1996; Clements *et al.* 1996a). These surveys seem to show a strong luminosity and/or density evolution of *IRAS* sources, but it is difficult to extrapolate this trend to higher redshifts on a firm ground. In spite of its observational limits, *IRAS* has also revealed the existence of *IRAS* 10214+4724, a very peculiar, “hyperluminous” galaxy at $z = 2.286$ (Rowan-Robinson *et al.* 1991a), though this object is likely affected by lensing (Eisenhardt *et al.* 1996). It is expected that the

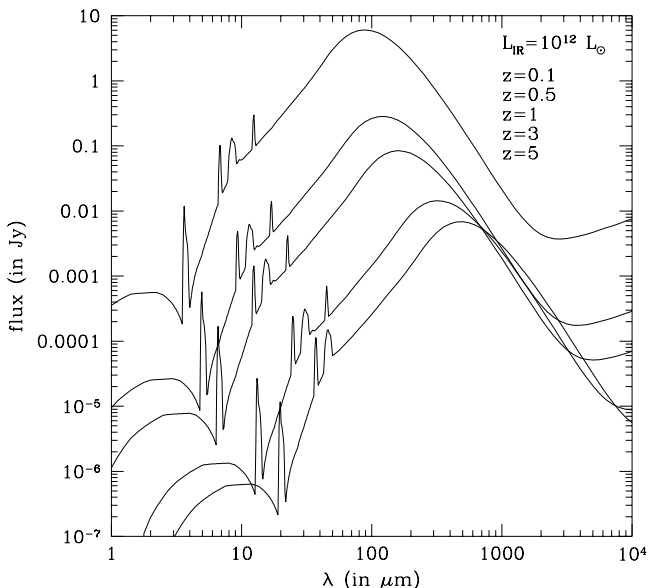


Figure 1. Observer-frame model spectra of a $L_{\text{IR}} = 10^{12} L_{\odot}$ galaxy at increasing redshifts (from top to bottom), for a cosmology with $h = 0.5$ and $\Omega_0 = 1$. The details of the modelling are explained in Sect. 3.2. The reader is invited to note that the apparent flux in the submm range is almost insensitive to redshift, because the shift of the 100 μm bump counterbalances the distance dimming.

ISO satellite will complete and detail this picture, in a broader wavelength range from a few μm to 200 μm . Other projects, such as *SIRTF*, will give access to better sensitivity and imaging capabilities.

The properties of galaxies in the submm range are sensitive to the spectral characteristics of dust, especially its emissivity at large wavelengths which is not constrained by *IRAS* observations alone. With respect to the relative wealth of data in the FIR, the submm emission of galaxies is poorly known. The observational literature gathers the submm fluxes of only a few tens galaxies which have been measured from ground-based or aircraft-borne instruments. These observations are difficult and some of the estimates of the amount of energy released in this range happen to be strongly discrepant (e.g. Chini *et al.* 1986; Stark *et al.* 1989; Eales *et al.* 1989; Chini and Krügel 1993). However, the observational situation will soon evolve with the start of SCUBA operations (and later, with SOFIA and especially *FIRST*). About twenty counterparts of radiogalaxies and quasars have already been observed at submm/mm wavelengths (see e.g. Hughes *et al.* 1997; and references therein). Although their evolutionary status is not fully understood, these objects give a first flavour of the future deep surveys which will be achieved by forthcoming instruments.

Theoretical modelling is needed to optimise observational strategies and also to help assess the point source contribution of the forthcoming CMB satellites MAP, and especially *PLANCK*. These experiments aim at mapping the anisotropies of the submm/mm sky on scales well below the degree. On these scales, the separation of the various fore-

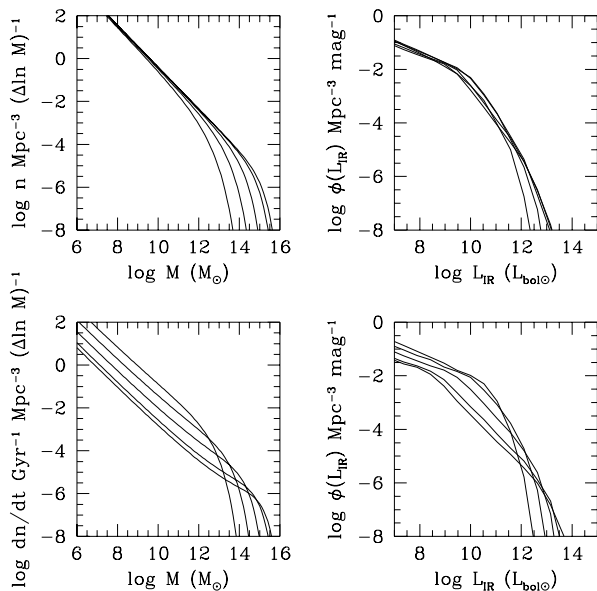


Figure 2. Number density and formation rate of collapsed haloes, and their relation to two modes of star formation. The left-hand panels show the number density of collapsed haloes (top) and the formation rate of collapsed haloes (bottom) computed for the SCDM model with $h = 0.5$, $\Omega_0 = 1$ and $\sigma_8 = 0.67$. The curves are plotted for redshifts $z = 3.67, 1.99, 0.92, 0.23$ and 0 (for increasing number densities at the high-mass end). The right-hand top panel shows the evolution of the IR luminosity function at the same redshifts, in the so-called “quiescent” mode of star formation with $\beta = 100$, $\alpha = 5$ and $V_{hot} = 130 \text{ km s}^{-1}$. The increase of the number of galaxies at all masses, as time goes on, is similar to the increase of the number of haloes and reflects the accumulation of galaxies. The right-hand bottom panel shows the evolution of the IR luminosity function at the same redshifts, in the so-called “burst” mode of star formation with $\beta = 10$. The galaxies undergo strong starbursts which act as beacons at the epochs of their initial collapses. Consequently, the evolution of the luminosity function reflects the formation rate of new haloes, with the characteristic crossing of the luminosity functions between low and high masses.

grounds and backgrounds which superimpose to the fluctuations of the CMB is more difficult than for the 7° field of view of the very successful *COBE*/DMR experiment. In the case of *PLANCK*, preliminary studies have shown that several thousands of galaxies should be detected at several wavelengths between $400 \mu\text{m}$ and 1 cm .

The epoch of galaxy formation can also be observed by its imprint on the background radiation which is produced by the line-of-sight accumulation of extragalactic sources. The search for the “Cosmic Optical Background” (hereafter COB) currently gives only upper limits. Nevertheless, the shallowing of the faint counts obtained in the HDF suggests that we are now close to convergence (Williams *et al.* 1996). Thus the lower limit to the COB obtained by summing up the contributions of faint galaxies is likely close to the real value. At longer wavelengths, the DIRBE instrument on *COBE* has given upper limits on the FIR background between 2 and $300 \mu\text{m}$ (Hauser 1995), while Puget

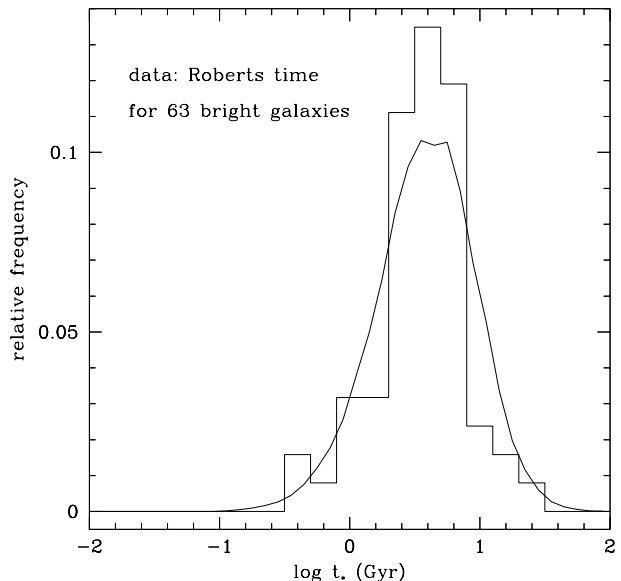


Figure 3. Distribution of the characteristic SFR time scales for the “quiescent” mode of star formation ($\beta = 100$, $V_{hot} = 130 \text{ km s}^{-1}$ and $\alpha = 5$). Only galaxies with $V_c > V_{hot}$ are retained. The histogram shows the data for a sample of 63 bright disk galaxies analysed by Kennicutt *et al.* (1994).

et al. (1996) have discovered an isotropic component in the *COBE*/FIRAS residuals between $200 \mu\text{m}$ and 2 mm , which could be the long-sought “Cosmic Infrared Background” (hereafter CIB). The presence of this component is confirmed by a new analysis restricted to the cleanest regions of the sky, where the foreground Galactic components are negligible (Guiderdoni *et al.* 1997). Such a detection seems to yield the first “post-*IRAS*” constraint on the high- z evolution of galaxies in the IR/submm range, before the era of *ISO* results. Its level comparable to the above-mentioned estimate of the COB suggests that a significant fraction of the energy of young stars is absorbed by dust and released in the IR/submm.

The models which have been proposed to predict the faint counts and background radiation in the IR/submm can be classified as “backward evolution” and “forward evolution”, following the good review by Lonsdale (1996). In the first class of models, the IR/submm luminosity function undergoes luminosity and/or number evolution which are simply parameterized as power laws of $(1+z)$ (e.g. Weedman 1990; Beichman and Helou 1991; Hacking and Soifer 1991; Oliver *et al.* 1992; Treyer and Silk 1993; Blain and Longair 1993; Pearson and Rowan-Robinson 1996). These power laws are generally derived from fits of *IRAS* galaxy counts (which do not probe deeper than $z \simeq 0.2$). Then they are extrapolated up to redshifts of a few units. Unfortunately, various analyses of *IRAS* deep counts yield discrepant results at $S_{60} < 300 \text{ mJy}$, and the issue of the evolution is very controverted (see e.g. Bertin *et al.* 1997, for a new analysis and discussion).

In the second class of models, the photometric evolution in the IR/submm is computed by implementing some

of the involved physical processes. For instance: chemical evolution which rules the amount of dust responsible for the IR/submm emission is modelled in Wang (1991a,b), and Eales and Edmunds (1996a,b). In addition to chemical evolution, the photometric evolution of stellar populations which heat the dust is modelled by Franceschini *et al.* (1991, 1994) and Fall, Charlot and Pei (1996). While the previous models assume a simple relation between the dust content and the heavy-element abundance of the gas, Dwek and Varosi (1996) try to explicitly model the processes of dust formation and destruction. However, both classes of models assume that all galaxies form at the same redshift z_{for} and that there is no number evolution. But the paradigm of the hierarchical growth of structures implies that there is no clear-cut redshift z_{for} since galaxy formation is a continuous process. Only Blain and Longair (1993a,b) proposed a formalism to compute the redshift range of galaxy formation, in addition to chemical evolution,

A consistent approach to the early evolution of galaxies is particularly important for any attempt at predicting their submm properties. Fig. 1 shows *model* spectra of a luminous IR galaxy as it would be observed if placed at different redshifts. There is a wavelength range, between $\sim 600 \mu\text{m}$ and $\sim 4 \text{ mm}$, in which the distance effect is counterbalanced by the “negative k-correction” due to the huge rest-frame emission maximum at $\sim 100 \mu\text{m}$. In this range, the apparent flux of galaxies depends weakly on redshift to the point that, evolution aside, a galaxy might be easier to detect at $z = 5$ than at $z = 0.5$! The observer-frame submm fluxes, faint galaxy counts and diffuse background of unresolved galaxies are consequently very sensitive to the early stages of galaxy evolution. Note that this particular wavelength range brackets the maximum of emission of the CMB.

The dissipative and non-dissipative processes ruling galaxy formation in dark matter haloes have been studied by various authors (see especially White and Rees 1978; Schaeffer and Silk 1985; Evrard 1989; Cole 1991; Blanchard *et al.* 1992). The modelling of these processes, complemented by star formation, stellar evolution and stellar feedback to the interstellar medium, has been achieved at various levels of complexity, in the so-called *semi-analytic* approach which has been successfully applied to the prediction of the statistical properties of galaxies (White and Frenk 1991; Lacey and Silk 1991; Lacey *et al.* 1993; Kauffmann *et al.* 1993, 1994; Cole *et al.* 1994; Heyl *et al.* 1995; Kauffmann 1995, 1996; Baugh *et al.* 1996a,b, 1997). It turns out that, in spite of differences in the details of the models, these studies lead to conclusions in the UV, visible and (stellar) NIR which are remarkably similar.

None of these models has been applied so far to the prediction of the properties of galaxies in the IR and submm ranges. This is the main aim of this paper which proposes a simple version of the semi-analytic approach and gives predictions of faint counts at wavelengths between $60 \mu\text{m}$ and 1.4 mm . This first study also intends to identify some of the difficulties arising in such a modelling. Sec. 2 quickly reviews the main physical processes which have to be introduced in order to describe the formation of galaxies: the non-dissipative collapse of perturbations, the dissipative collapse of the gas, star formation and evolution, and feedback. Sec. 3 addresses the peculiar issue of dust absorption and re-emission in the IR and submm. Sec. 4 extracts useful infor-

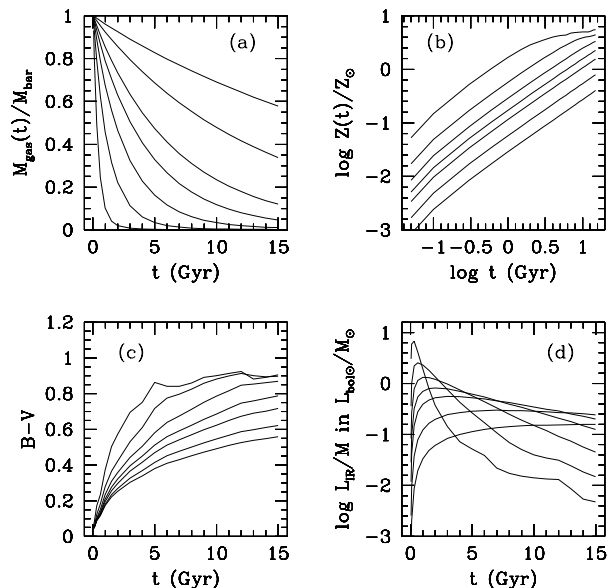


Figure 4. Evolution of various quantities for a grid of models with $t_{\star} = 0.33, 1, 2, 3, 5, 10$ and 20 Gyr. Panel *a*: gas fraction (from bottom to top). Panel *b*: gas metallicity (from top to bottom). Panel *c*: $B-V$ colour (from top to bottom, taking into account face-on internal extinction). Panel *d*: luminosity re-emitted by dust in the IR/submm (from top to bottom at 1 Gyr).

mation from the recent UV/visible deep surveys and uses the new constraint arising from the CIB in order to generate a family of evolutionary scenarios. Sec. 5 gives the IR/submm counts predicted from these scenarios. Finally, Sec. 6 briefly discusses these results, as well as the shortcomings of such models, and concludes.

In a previous study, we showed that the CIB can be disentangled with a family of evolutionary scenarios which predict steep submm counts, and that the observations with *ISO* (at $175 \mu\text{m}$) will soon constrain the IR/submm evolution at $z \sim 1$ and beyond (Guiderdoni *et al.* 1997). Here we present the details of the modelling and apply it to other observations, more specifically in SCUBA bands (through the narrow submm atmospheric windows). A preliminary version of this work was presented in Guiderdoni *et al.* (1996). A forthcoming paper (Hivon *et al.* 1997) will show simulations of the anisotropies of the diffuse submm background due to galaxies and will study the possibility of their detection, with current and forthcoming instruments. Other papers in this series will try to overcome some of the shortcomings of this first study.

2 A SCHEMATIC VIEW OF GALAXY FORMATION

2.1 Non-dissipative collapse

The formation and evolution of a galaxy in its dark matter halo can be briefly sketched as follows: the initial perturbation, which is gravitationally dominated by non-baryonic dark matter, grows and collapses. After the (non-dissipative)

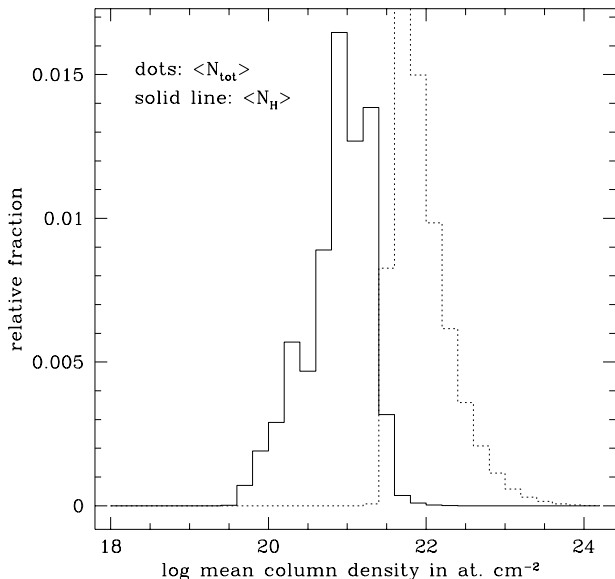


Figure 5. Distribution of mean column densities at $z = 0$, in atom cm^{-2} , for galaxies with $SB_e < 25 \text{ mag arcsec}^{-2}$, and the “quiescent” mode of star formation ($\beta = 100$, $\alpha = 5$ and $V_{hot} = 130 \text{ km s}^{-1}$). Dotted line: $\log < N_{tot} >$; solid line: $\log < N_H >$.

collapse, and subsequent violent relaxation, the halo virializes, through the formation of a mean potential well seen by all particles, which consequently share the same velocity distribution. As detailed in the Appendix, we use the classical top-hat model for spherically-symmetric perturbations, and we compute the mass distribution of collapsed haloes from the peaks formalism (Bardeen *et al.* 1986), as in Lacey and Silk (1991) and Lacey *et al.* (1993). Hereafter, we shall consider the SCDM model with $H_0 = 50 \text{ km s}^{-1} \text{ Mpc}^{-1}$, $\Omega_0 = 1$, $\Lambda = 0$, and $\sigma_8 = 0.67$ as an illustrative case. We take a baryonic fraction $\Omega_{bar} = 0.05$, consistent with primordial nucleosynthesis. The redshift evolution of the number density and formation rate of collapsed haloes is plotted in fig. 2.

2.2 Cooling and dissipative collapse

The baryonic gas cools in the potential wells of dark matter haloes, by a process identical to cooling flows observed at the centre of rich clusters. The cooling time at halo radius r is

$$t_{cool}(r) = \frac{3}{2} \frac{n_{tot}(r) k T_V}{n_e^2(r) \Lambda(T_V)} = 3\pi G \mu_e^2 m_p^2 \frac{\Omega_0}{\Omega_{bar}} \frac{r^2}{\Lambda(T_V)}, \quad (1)$$

with $\mu_e = 1.14$ for ionized primordial gas. The cooling curve $\Lambda(T)$ takes into account various cooling processes. We do not consider the metallicity dependence of $\Lambda(T)$. Neglecting this dependence leads to an *overestimate* of cooling times, which are already very short. The equation $t_{cool}(r_{cool}) = t(z)$ defines a cooling radius r_{cool} as a function of redshift z . At this redshift, only gas inside r_{cool} (or r_V if $r_{cool} > r_V$) cools and is available for star formation. This cooling criterion introduces a high-mass cut-off in the mass distribu-

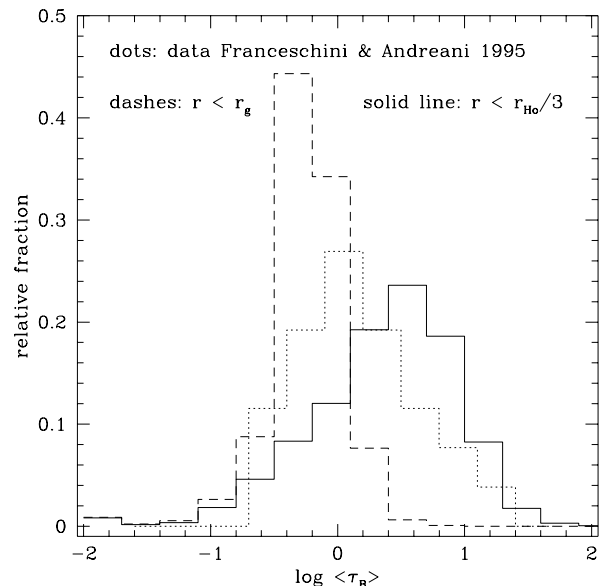


Figure 6. Distribution of mean, face-on optical depth in the B -band at $z = 0$, for the “quiescent” mode of star formation ($\beta = 100$, $\alpha = 5$ and $V_{hot} = 130 \text{ km s}^{-1}$). Two ways of computing τ_B are considered. Dashes: Mean optical depth inside the gas radius ($r_g = 1.6r_{25}$). Solid line: Mean optical depth inside one third of the Holmberg radius (at $26.5 \text{ mag arcsec}^{-2}$). The dotted line shows the observational distribution in a sample of normal spirals and luminous IR galaxies from Franceschini and Andreani (1995). The total dust quantity derived from 1.3 mm observations is distributed within one third of the Holmberg radius and an observational estimate of τ_B is computed. The observational distribution peaks at the value $< \tau_B > \sim 1$ and is bracketted by the two predicted histograms.

tion of cold baryonic cores. At the low-mass end, the cooling is so efficient that almost all the gas can cool, leading to a slope of the mass distribution of baryonic cores $n(M_{bar})dM_{bar} \propto M_{bar}^{-1.95}dM_{bar}$ at redshift $z = 0$, which is close to the slope $n(M)dM \propto M^{-2}dM$ for the number density of collapsed haloes. This is the so-called “overcooling” problem (Cole 1991; Blanchard *et al.* 1992).

The final radius of the cold gas in rotational equilibrium is related to the initial radius by conservation of angular momentum (Fall and Efstathiou 1980). Approximately, $r_D \sim \lambda \min(r_V, r_{cool})$, with the dimensionless spin parameter $\lambda \equiv J|E|^{1/2}G^{-1}M^{-5/2} \simeq 0.05 \pm 0.03$ (Barnes & Efstathiou 1987; Efstathiou *et al.* 1988; Zurek *et al.* 1988). Previous studies only used the mean value of λ in this formula. Hereafter, we introduce the λ distribution from Barnes and Efstathiou (1987) model C0-4 (their fig. 11). According to a fit based on fig. 3 of Fall and Efstathiou (1980), the exponential disk which forms from the dissipative collapse of the gas has a length scale $r_0 \simeq 1.26\lambda^{1.17} \min(r_V, r_{cool})$ and a radius including half the cold baryonic mass $r_{1/2}/r_0 = 1.68$. A dynamical time scale in the disk-like core is $t_{dyn} \equiv 2\pi r_{1/2}/V_c$. It is important to note that only disks can form in this formalism. The formation of elliptical galaxies (and of bulges of spiral galaxies) has to be explained by the merging of disks. Kauffmann *et al.* (1993) and Cole *et al.* (1994) showed that

this merging process can easily explain the current fraction of gE among bright galaxies.

2.3 Star formation

Locally, the SFR depends on numerous physical parameters. Nevertheless, phenomenological studies seem to show that, on galaxy scales, the SFR per unit surface density is proportional to the total gas surface density (neutral plus molecular) divided by the dynamical time scale of the disk (Kennicutt 1989, 1997). So we shall hereafter assume that the star formation time scale t_* is proportional to the dynamical time scale of the disk t_{dyn} and we introduce a first efficiency factor β . With $t_* \equiv \beta t_{dyn}$, we take:

$$SFR(t) = \frac{M_{gas}(t)}{t_*}. \quad (2)$$

Fig. 3 shows the predicted t_* histogram compared to the histogram of “Roberts times” for a sample of 63 bright disk galaxies observed by Kennicutt *et al.* (1994). The Roberts time is defined as $t_R \equiv (M_{HI} + M_{H_2})/SFR(t_0)$ where M_{HI} is the gas mass in the HI phase measured from the 21 cm line, M_{H_2} is the gas mass in the H₂ phase measured from the CO line, and $SFR(t_0)$ is the total star formation rate measured from the H α line, under an assumption about the shape of the Initial Mass Function (hereafter this is Salpeter IMF). The interesting result is that the model correctly predicts the *shape* and *width* of the histogram. We emphasize that this agreement is due to both the range of halo densities (scaling as $(1 + z_{coll})^3$) and dimensionless spin parameters λ . Without the λ scatter, the predicted distribution would be about three times too narrow. The average value of the observed histogram can be reproduced by taking $\beta \simeq 100$ for our SCDM model.

Finally, for sake of simplicity, we use a Salpeter IMF with index $x = 1.35$. Stars have masses $0.1 \leq m \leq 120 M_\odot$. We also assume that the mass fraction blocked in dark objects with masses below $0.1 M_\odot$ is negligible.

2.4 Stellar feedback

The explosion of massive stars can expel gas from the galaxies and quench star formation, leading to a strong increase of the mass-to-luminosity ratios in small objects. Observationally, HI holes and X-ray superbubbles are good evidence that such galactic winds are present in galaxies. The stellar feedback is introduced in a similar way by most authors, following the original work by Dekel and Silk (1986). By equating the gas binding energy to the thermal energy ejected by supernovae, one gets:

$$\frac{1}{2} M_{gas}(t) \left(\frac{V_{esc}}{V_c} \right)^2 V_c^2 = \epsilon \int_0^{t_W} \tau_*(t') \eta_{SN} E_{SN} dt', \quad (3)$$

where η_{SN} is the number of SNe per unit mass of stars, depending on the IMF. For our choice of IMF, $\eta_{SN} = 7.4 \cdot 10^{-3} M_\odot^{-1}$. The output mechanical energy of a SN is $E_{SN} \sim 10^{51}$ erg. The escape velocity at radius $r \leq r_V$ in a singular isothermal sphere truncated at radius r_V is $V_{esc}(r) = \sqrt{2} V_c (1 - \ln(r/r_V))^{1/2}$. The maximum of the λ distribution corresponds to $r_{1/2}/r_V \simeq 0.05$, leading to $V_{esc}/V_c \simeq 2.8$. Since much of this energy is subsequently radiated away, we insert a second efficiency factor $0 \leq \epsilon \leq 1$. After some

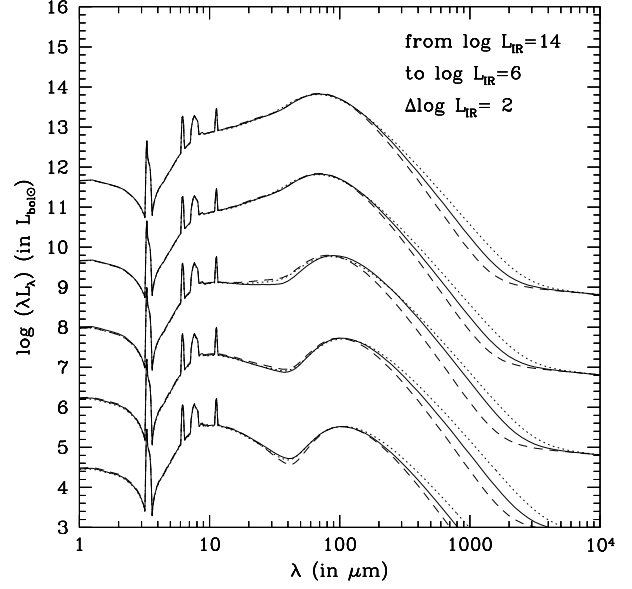


Figure 7. Model spectra in the IR and submm, for IR luminosities 10^6 , 10^8 , 10^{10} , 10^{12} , and $10^{14} L_{bol\odot}$. Emissivity index of big grains: $m = 2$ (dashes), $m = 1.5$ (solid lines), $m = 1$ (dotted lines).

algebra, the mass fraction of stars F_* forming before the triggering of the galactic wind at time t_W is given by:

$$F_* \equiv \frac{M_*(t_W)}{M_*(t_W) + M_{gas}(t_W)} = (1 + (V_{hot}/V_c)^\alpha)^{-1}, \quad (4)$$

with $\alpha = 2$ and $V_{hot} \equiv (V_c/V_{esc})(2\eta_{SN}E_{SN})^{1/2}\epsilon^{1/2} = 310 \epsilon^{1/2} \text{ km s}^{-1}$ for the Salpeter IMF. Nevertheless, there is much uncertainty on these parameters because of the cooling of supernova remnants before wind triggering. For instance, numerical simulations seem to suggest that $\epsilon \sim 0.1$ (Thorn-ton *et al.* 1997). Cole *et al.* (1994) introduced a fit based on SPH simulations of galaxy formation in which most of the feedback effect is due to momentum exchange rather than to ISM heating (Navarro and White 1993). For a typical feedback parameter $f_V = 0.1$, the numerical simulations can be fitted with $\alpha = 5$ and $V_{hot} = 130 \text{ km s}^{-1}$. We shall hereafter take these values as our standard parameters. The situation is still complicated by the existence of *non-local* feedback processes in addition to the local ones. Efstathiou (1992) and Blanchard *et al.* (1992) suggest that high- z re-ionization of the IGM could prevent cooling in haloes with circular velocities below $V_{equ} \sim 20$ to 50 km s^{-1} , and possibly as high as $\sim (200)^{1/3} V_{equ}$ in case of adiabatic collapse. So it is very likely that the overall quenching of dwarf formation depends on redshift. Introducing this redshift dependence of dwarf formation partly alleviates the problem of the steep slope of the luminosity function (see e.g. Kauffmann *et al.* 1993). So the situation appears to be very complicated, in the absence of a global theory of feedback processes. In the following, we shall simply model the combination of local and non-local feedbacks by introducing a simple $(1 + z_{coll})$ dependence for V_{hot} .

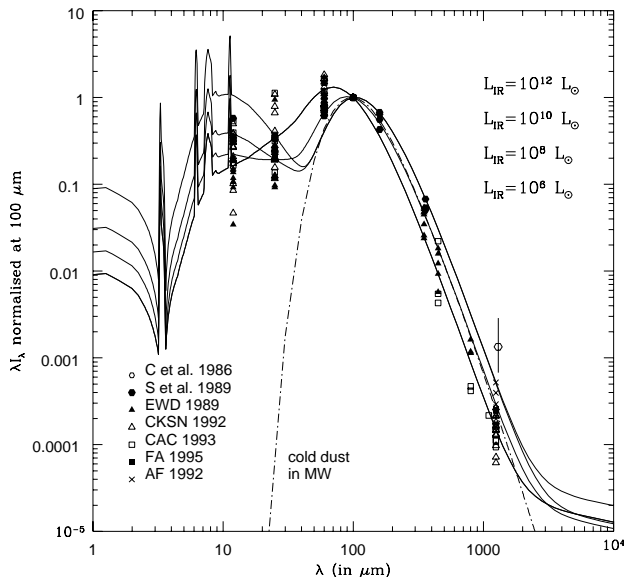


Figure 8. Model spectra with $m = 1.5$ superimposed to a compilation of data in the FIR and submm: Chini *et al.* 1986 (mean value), Stark *et al.* 1989, Eales *et al.* 1989, Carico *et al.* 1992, Andreani and Franceschini 1992, Clements *et al.* 1993, Franceschini and Andreani 1995 (mean value). The dashes-and-dots show a typical spectrum of cold dust in the Milky Way (Reach *et al.* 1995). Models and data are normalised at $100 \mu\text{m}$.

2.5 Spectral evolution of the stellar population

A model of spectrophotometric evolution is used to compute the age dependence of the gas content, the UV to NIR spectra of the stellar populations, and the mass-to-luminosity ratios. The stars are placed on the Zero-Age Main Sequence of the HR diagram according to the IMF. The models use compilations of stellar evolutionary tracks taking into account the various stages of stellar evolution in order to compute at each time step the distribution of stellar populations in the HR diagram. This distribution is combined with a library of stellar spectra and gives the synthetic spectrum F_{λ} . At the end of their lifetimes, stars die and return a fraction of their mass to the ISM. The model which is used here is described in Guiderdoni and Rocca-Volmerange (1987, 1988), and Rocca-Volmerange and Guiderdoni (1988), and includes upgraded stellar tracks from Schaller *et al.* (1992) and Charbonnel *et al.* (1996).

Panel *a* of fig. 4 shows the grid of models with various t_* from 0.33 to 20 Gyr, which are introduced in order to follow the relative gas content of the galaxy $g(t) \equiv M_{\text{gas}}(t)/M_{\text{bar}}$. The heavy elements synthesised by stars are injected into the interstellar medium. The metallicity of the gas is estimated from the Instant Recycling Approximation $Z_g(t) = -yz \ln g(t)$ with a yield yz depending on the choice of the IMF. Panel *b* shows the time variation of $Z_g(t)$ for the grid of models. The photometric properties can be computed after taking into account the intrinsic extinction (see the following section). As an example, panel *c* gives the face-on $B-V$ colours.

2.6 The slope of the luminosity function

Before examining the modelling of the IR emission of galaxies, we would like to quickly comment on the slopes of the B -band luminosity and gas mass functions obtained by this simple version of the semi-analytic approach.

In spite of the variety of SFR histories, and of the strong variation of the mass-to-luminosity ratios in time scales of a few Gyr, the *shape* of the luminosity function in the absence of feedback processes is surprisingly similar to that of the baryonic mass function. For $\phi(L_B)dL_B \propto L_B^s dL_B$, our model with $\beta = 100$ and the standard mass loss ($\alpha = 5$ and $V_{\text{hot}} = 130 \text{ km s}^{-1}$) gives $s = -1.4$, whereas Loveday *et al.* (1992) find $s = -1$. Such an uncomfortable situation is a robust result of *all* the recent attempts to model galaxy formation and evolution in a semi-analytic approach (see Kauffmann *et al.* 1994; Cole *et al.* 1994). Although it seems in disagreement with the nearby surveys (but other surveys seem to suggest an increase of the slope at the faint end, e.g. Marzke *et al.* 1994), this steep slope is necessary to reproduce the deep redshift surveys (down to $B_J < 24$) and the faint galaxy counts (down to $B_J < 28$). Subtle selection effects due to surface brightness could explain the discrepancy between the nearby luminosity function and the high- z one (McGaugh 1994; Lobo and Guiderdoni 1997).

Indeed, this type of selection effect can be suspected because the predicted gas mass function is in better agreement with the observational data. The predicted mass distribution of gas at redshift $z = 0$ has a slope $n(M_{\text{gas}})dM_{\text{gas}} \propto M_{\text{gas}}^{-1.3} dM_{\text{gas}}$ (with the standard values or the parameters). Smaller objects form earlier on an average, with higher densities, smaller t_{dyn} , smaller t_* , and, consequently, they are more affected by mass loss and their relative gas content is lower. It is possible to correct statistically the total gas mass function in order to predict an HI mass function and compare it to the observational slope -1.35 determined by Briggs and Rao (1993). In the sample of 63 disk galaxies gathered by Kennicutt *et al.* (1994), there is no systematic trend for $M_{\text{HI}}/M_{\text{gas}}$ versus M_{gas} , t_R , or the *SFR*. We have made an histogram of $\log(M_{\text{HI}}/M_{\text{gas}})$, with values from -1 to 0 , and we have distributed the predicted number density at M_{gas} into the range of M_{HI} values according to this histogram. The effect of this correction turns out to be rather small. Thus there is a good agreement of the predictions with the observations. It is worthwhile to emphasize that the slope -1.35 of the data depends on the volume corrections of the survey for low-mass objects and is somewhat uncertain.

3 SPECTRAL EVOLUTION OF DUST EMISSION

3.1 Dust absorption

Part of the energy released by stars is absorbed by dust and re-emitted in the IR and submm ranges. The derivation of the IR/submm spectrum is a three-step process: i) computation of the optical thickness of the disks; ii) computation of the amount of bolometric energy absorbed by dust; iii) computation of the spectral energy distribution of dust emission. The modelling of these steps is not an easy task since it requires addressing confused issues such as the chem-

Table 1. Scenarios of galaxy evolution

Name	f_{burst} ($\beta = 10$)	$f_{quiescent}$ ($\beta = 100$)	% of ULIGs	Line code
Q	0	1	0 %	dots and small dashes
A	$0.04(1 + z_{coll})^5$	$1 - f_{burst}$	0 %	solid line
B	$0.04(1 + z_{coll})^5$	$1 - f_{burst}$	5 % at all z_{coll}	dotted line
C	$0.04(1 + z_{coll})^5$	$1 - f_{burst}$	90 % for $z_{coll} > 3.5$	long dashes
D	$0.04(1 + z_{coll})^5$	$1 - f_{burst}$	15 % at all z_{coll}	short dashes
E	$0.04(1 + z_{coll})^5$	$1 - f_{burst}$	$1 - \exp -0.02(1 + z_{coll})^2$	dots and long dashes

ical evolution of the dust, and the geometrical distribution of dust relatively to stars.

We assume that the gas is distributed in an exponential disk with truncation radius r_g and mean H column density $< N_H(t) > = M_{gas}(t)/1.4m_H\pi r_g^2$. The factor 1.4 accounts for the presence of helium. If r_{25} is the isophotal radius at 25 mag arcsec⁻², the observations give $r_g/r_{25} \simeq 1.6$ (Bosma 1981). The r_{25} radii are consistently computed from the B magnitudes and r_0 radii of the galaxies. Fig. 5 shows the mean total and gas surface densities inside r_g at redshift $z = 0$. These surface densities fairly correspond to the crude estimate $< N_H(t) > = 6.8 \cdot 10^{21} g(t)$ atom cm⁻² used in Guiderdoni and Rocca-Volmerange (1987) and Franceschini *et al.* (1991, 1994). As noted by Guiderdoni & Rocca-Volmerange (1987), a galaxy with $g \simeq 0.20$ has an H column density $< N_H > \simeq 1.4 \cdot 10^{21}$ atom cm⁻² in good agreement with the observational value for late-type disks, in spite of the uncertainties in this estimate (Guiderdoni 1987).

The mean optical thickness inside r_g is given by:

$$\tau_\lambda(t) = \frac{1}{1.086} \frac{A_\lambda}{A_V} (Z_g(t)) \frac{A_V}{E_{B-V}} \frac{E_{B-V}}{N_H} < N_H(t) > \quad (5)$$

$$= \left(\frac{A_\lambda}{A_V} \right)_{Z_\odot} \left(\frac{Z_g(t)}{Z_\odot} \right)^s \left(\frac{< N_H(t) >}{2.1 \cdot 10^{21} \text{ at cm}^{-2}} \right). \quad (6)$$

As in Guiderdoni and Rocca-Volmerange (1987) and Franceschini *et al.* (1991, 1994), the extinction curve depends on the gas metallicity $Z_g(t)$ according to power-law interpolations based on the Solar Neighbourhood and the Magellanic Clouds, with $s = 1.35$ for $\lambda < 2000$ Å and $s = 1.6$ for $\lambda > 2000$ Å. The extinction curve for solar metallicity is taken from Mathis *et al.* (1983).

It is not clear whether the disks of “normal” spirals are optically thin or optically thick. Catalogues of galaxies (such as the classical RC2 and the RSA) suggest $\tau_B = 0.7$ for spirals. On the other hand, several studies have pointed out the possibility of optically-thick disks (see e.g. Disney *et al.* 1989 and references therein). Since the gas decrease is counterbalanced by the metallicity increase, the optical thickness of our grid of models is maximal for $g(t) = e^{-s} \simeq 0.20$ with $s = 1.6$. Late-type disks spend most of their life time at optical depths $\tau_B \simeq 0.4 - 0.7$, in good agreement with what is suggested in the RC2 or RSA, and with the estimates of Rowan-Robinson (1992) based on *IRAS* results. Fig. 6 gives the predicted distribution of optical thicknesses which fairly compares with a sample of normal spirals and luminous IR galaxies (Franceschini and Andreani 1995).

As in Guiderdoni and Rocca-Volmerange (1987) and Franceschini *et al.* (1991, 1994), we also assume a simple geometric distribution where the gas and the stars which

contribute mainly to dust heating are distributed with equal height scales in the disks. If $\tau_\lambda(t)$ is the optical thickness of the disks at wavelength λ and time t , the extinction correction (averaged over inclination angle i) is:

$$A_\lambda(t) = -2.5 \log < \frac{1 - \exp(-a_\lambda \tau_\lambda(t)/\cos i)}{a_\lambda \tau_\lambda(t)/\cos i} >_i, \quad (7)$$

providing that the stars and gas have the same height scales. The factor $a_\lambda \equiv (1 - \omega_\lambda)^{1/2}$ crudely takes into account the effect of the albedo ω_λ (from Draine and Lee 1984) for isotropic scattering (Natta and Panagia 1984) and relates extinction to absorption. This “slab” geometry is intermediate between the “screen” geometry $\exp -a_\lambda \tau_\lambda / \cos i$ and the “sandwich” geometry (with zero height scale for dust) $(1 + \exp -a_\lambda \tau_\lambda / \cos i)/2$ which respectively lead to larger and smaller absorption. Observational analyses seem to suggest that this “slab” geometry is the best guess to fit the data (see e.g. Franceschini and Andreani 1995; Andreani and Franceschini 1996).

Finally, the bolometric luminosity which is absorbed by dust and released in the IR/submm is:

$$L_{IR}(t) = \int F_{\star\lambda}(t) (1 - 10^{-0.4A_\lambda(t)}) d\lambda. \quad (8)$$

Panel *c* and *d* of fig. 4 respectively show the face-on extinguished $B - V$ colours and the IR bolometric luminosities per unit mass of galaxy for a grid of models with various t_* . The corresponding range of IR-to-blue luminosity ratios $0.06 \leq L_{IR}/\lambda_B L_B \leq 4$ is very similar to the observed range for optically-selected samples, for instance the sample drawn from the Zwicky Catalogue with $m_z < 15.7$ mag in Soifer *et al.* (1987), and characterizes “mild starbursts” and LIGs. The IR-to-blue luminosity ratios are sensitive to τ_B and the geometry. If there are tidally-induced gas inflows resulting in smaller r_g and to a “screen”-like gas distribution, this ratio can easily reach 10–100 as in the ULIGs. We hereafter keep the LIG-type efficiency of conversion between the optical and the IR as a conservative estimate, and we shall consider the population of ULIGs in Sec. 4.3.

3.2 Dust emission

The emission spectra of galaxies are computed as a sum of various components, according to the method developed by Maffei (1994), which uses the observational correlations of the *IRAS* flux ratios $12\mu\text{m}/60\mu\text{m}$, $25\mu\text{m}/60\mu\text{m}$ and $100\mu\text{m}/60\mu\text{m}$ with L_{IR} (Soifer and Neugebauer 1991). These correlations are extended to low L_{IR} with the samples of Smith *et al.* (1987) and especially Rice *et al.* (1988).

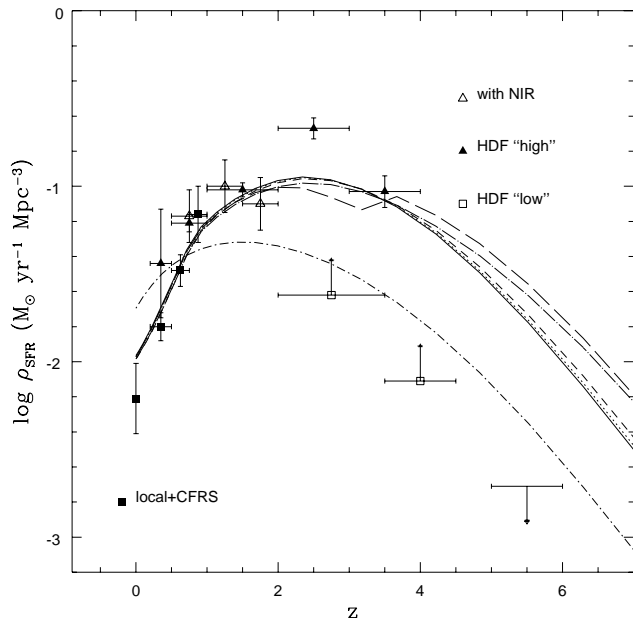


Figure 9. Evolution of the cosmic comoving star formation rate density as computed from rest-frame UV luminosity densities, by using Salpeter IMF with slope 1.35. The UV densities are based on the integration of the luminosity function fit on all magnitudes. The UV fluxes have *not* been corrected for intrinsic extinction. The solid squares are derived from the rest-frame 2800 Å luminosity density in the Canada-France Redshift Survey, and the local value is from the *B*-band luminosity function and average UV-*B* colour (Lilly *et al.* 1996). The open triangles take into account NIR data to compute photometric redshifts in the Hubble Deep Field (Connolly *et al.* 1997). The solid triangles come from another photometric-redshift analysis of the HDF (Sawicki *et al.* 1997), while the open squares with the arrows are lower and upper values from the HDF with redshifts derived from Lyman-continuum drop-outs (Madau *et al.* 1996). Scenario Q (“quiescent” mode, $\beta = 100$) is plotted with dots and small dashes. It is unable to reproduce the steep decline of ρ_{SFR} between redshifts 1 and 0. Other scenarios involve an increasing fraction of the “burst” mode ($\beta = 10$) with redshift, producing a population of LIGs. Scenario A (solid line) has no ULIGs. Various quantities of ULIGs are included in scenarios B (dotted line), C (long dashes), D (short dashes) and E (dots and long dashes). See tab. 1 for details and summary of lines codes. The SFRs slightly differ because t_* is considered as an exponential time scale for the LIGs and a burst duration for the ULIGs.

Several components are considered in the model spectra:

- Polycyclic aromatic hydrocarbons (PAH). Because of their small size (≤ 1 nm), these molecules never reach thermal equilibrium when they are excited in a UV/visible radiation field. Their temperature fluctuates and can reach a value much higher than the equilibrium temperature, explaining the 12 μ m excess and the bands at 3.3, 6.2, 7.7, 8.6 and 11.3 μ m. Their template emission spectrum is taken from the model by Désert *et al.* (1990).

- Very small grains (VSG). They are made of graphite and silicates. These dust grains have sizes between 1 and 10 nm. As the PAH, they never reach thermal equilibrium.

Consequently, their emission spectrum is much broader than a modified black body spectrum at a single equilibrium temperature. The template emission spectrum is also taken from the model by Désert *et al.* (1990).

- Big grains (BG). They are also made of graphite and silicates. These dust grains have sizes between 10 nm and 0.1 μ m. They (almost) reach thermal equilibrium and can be reasonably described by a modified black body $\epsilon_\nu B_\nu(T_{BG})$ and emissivity $\epsilon_\nu \propto \nu^m$ with $1 \leq m \leq 2$.

- Synchrotron radiation. This non-thermal emission is strongly correlated with stellar activity and, as a consequence, with IR luminosity (see e.g. Helou *et al.* 1985). According to observations at 1.4 GHz, this correlation is $L_\nu(1.4 \text{ GHz}) = L_{IR}/(3.75 \cdot 10^{12} \times 10^q)$. Here L_{IR} is in W, $\nu_{80} = 3.75 \cdot 10^{12}$ Hz is the frequency at 80 μ m and $q \simeq 2.16$ is determined from observations. Then we assume that we can extrapolate from 21 cm down to ~ 1 mm with a single average slope 0.7, so that $L_\nu = L_\nu(1.4 \text{ GHz})(\nu/1.4 \text{ GHz})^{-0.7}$.

The 60/100 colour gives the temperature T_{BG} of the BG, provided that an emissivity index m has been chosen. We hereafter test $m = 1, 1.5$ (standard value) and 2. Then the amount of BG, VSG and PAH are calculated iteratively from the 12/100, 25/100 and 60/100 ratios. The resulting spectra are computed from a few μ m to several mm and evolve with L_{IR} such as more luminous galaxies preferentially emit at shorter wavelengths. By construction, these spectra fit the *IRAS* colour correlations. Fig. 7 shows examples of these model spectra for various L_{IR} and three values of the emissivity index for BG.

In spite of its shortcomings, this method takes into account the observed spectral evolution in the IR and submm/mm ranges, while previous works generally use a single template spectrum in the whole spectral range. It is also possible to reproduce the FIR photometry of various individual galaxies by this method (Maffei 1994). Fig. 8 shows a compilation of data superimposed to a series of model spectra. The compiled samples gather galaxies which have been observed at least at one wavelength in the submm range, (say, between 200 μ m and 1.3 mm) with a positive detection. The various samples are very heterogeneous. They have been obtained with different telescopes and instruments and focus upon different types of galaxies (“normal” spirals, LIGs, ULIGs). None of them is complete. Moreover, there is very little overlap between the samples, and the few galaxies which have been observed by various authors with various instruments generally have discrepant fluxes. These discrepancies can originate from the choices of beam size and beam shopping. Andreani and Franceschini (1992, 1996) have studied the effect of the finite extension of the submm emission and computed an average aperture correction, which turns out to be rather small.

There is some debate about the presence of very cold dust which could emit at submm wavelengths. Chini *et al.* (1986), confirmed by Chini and Krügel (1993), claim that the dust seen at *IRAS* wavelengths is unable to reproduce the observed submm emission. On the contrary, Stark *et al.* (1989), Eales *et al.* (1989), and Clements *et al.* (1993) do not detect any evidence for this new component. Chini *et al.* (1986) interpret their high fluxes as an evidence for the existence of cold dust. The value of the derived temperature depends on the choice of the emissivity index of these grains,

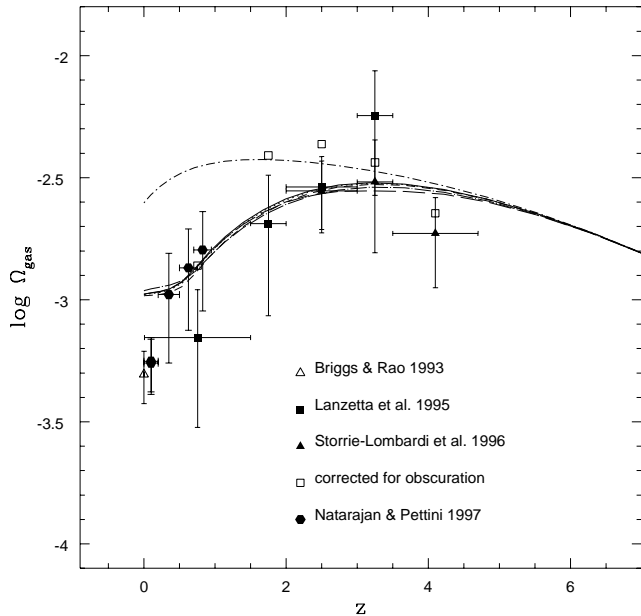


Figure 10. Evolution of the cold gas density parameter in damped Lyman- α absorbers. Solid squares: data without the APM QSO survey. Solid triangles: data including the APM QSO survey. Open squares: tentative correction for selection effects due to QSO obscuration (Storrie-Lombardi *et al.* 1996). Solid hexagons: Natarajan and Pettini (1997). Open triangle: local estimate from HI surveys (Briggs and Rao 1993). Line codes of scenarios Q, A, B, C, D, E are given in tab. 1. The various scenarios involving the “burst” mode consume more gas than the “quiescent” mode (dots and short dashes).

which can be anything between 1 and 2. Clearly, the uncertainties in the submm emission are large, and the need for a systematic survey of a complete sample is strong. There is no doubt that this will be one of the first targets of SCUBA. Because of these uncertainties, the models with an average index $m = 1.5$ plotted in fig. 8 seem to cover the range of observations at submm wavelengths, except the high fluxes observed by Chini *et al.* (1986).

4 THE HISTORY OF STAR FORMATION IN THE UNIVERSE

4.1 The “quiescent” mode of star formation

In this section, we will introduce scenarios of evolution which will be used to compute the IR/submm properties of galaxies, and to predict faint galaxy counts, and the CIB. The description of these scenarios and their line codes in the figures are summarized in tab. 1. While a complete assessment of the energy budget of galaxies would require the monitoring of multi-wavelength luminosity functions and galaxy counts (delayed to forthcoming studies), we hereafter only wish to address the issue of the overall evolution of the comoving SFR and gas densities in the universe. Pei and Fall (1995) and Fall *et al.* (1996) emphasized the relevance of these quantities to describe the overall evolution of the galaxy population.

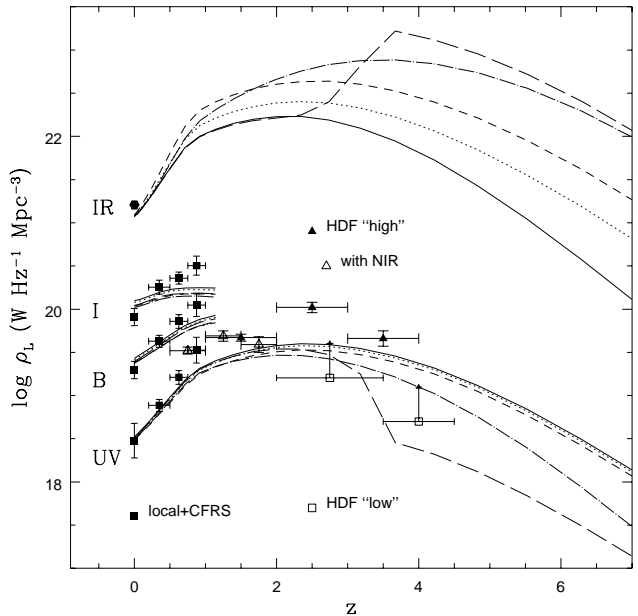


Figure 11. Rest-frame comoving luminosity density. Letters UV, B, I and IR respectively stand for 2800 Å, 4400 Å, 10000 Å and 60 μ m. The emissivity at 1600 Å is about 30 % higher than at 2800 Å. The luminosity densities are based on the integration of the luminosity function fit on all magnitudes. Solid squares: local and Canada-France Redshift Survey (Lilly *et al.* 1996). Open triangles: NIR data are taken into account to compute photometric redshifts in the Hubble Deep Field (Connolly *et al.* 1997). Solid triangles: other estimates of photometric redshifts in the HDF (Sawicki *et al.* 1997). Open squares with arrows: HDF with redshifts from Lyman-continuum drop-outs (Madau *et al.* 1996). Solid hexagon: 60 μ m local density corresponding to one third of the bolometric light radiated in the IR (Saunders *et al.* 1990). Line codes of scenarios A, B, C, D, E are given in tab. 1. The different UV and IR emissions mainly result from different fractions of ULIGs (with a top-heavy IMF and strong extinction), with almost similar SFR histories. Strongly differing high- z IR emission are obtained without being much constrained by the current status of (discrepant) UV/optical observations.

Fig. 9 and 10 respectively show the predicted SFR and gas evolutions for scenario Q with $\beta = 100$. It corresponds to the fit of SFR time scales in disks, that is, the so-called “Roberts times” peaking at 3 Gyr and ranging between 0.3 and 30 Gyr (Kennicutt *et al.* 1994). The feedback parameters are $\alpha = 5$ and $V_{hot} = 40(1 + z_{coll})$ km s $^{-1}$. This somewhat arbitrary $(1 + z)$ dependence is intended to mimic the effect of global re-heating at high redshift and avoids a step-wise change of V_{hot} at $z = 2$ caused by a bimodal regime. This has almost no effect at low z but it changes the high-redshift behaviour of the SFR density.

Clearly the SFR density in scenario Q does not decline fast enough between $z = 1$ and the local universe, and, correspondingly, gas is not consumed sufficiently. The impossibility to reproduce the peak of SFR density with star formation histories similar to those in disks is not surprising. We know that their present SFR time scales (the Roberts times) are large and that their SFRs have not changed significantly during the last few billion years (Kennicutt *et al.* 1994).

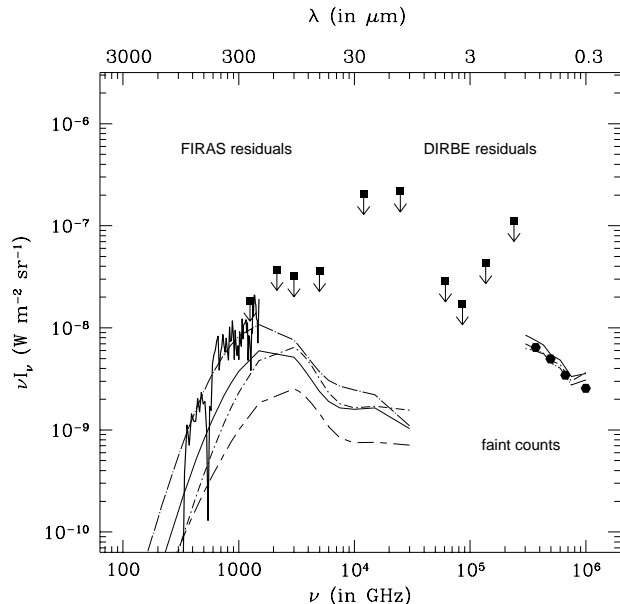


Figure 12. Predictions of the diffuse backgrounds in the FIR/submm and in the optical compared to the current upper limits and detections. The solid squares show the level of COBE/DIRBE residuals from Hauser (1995). The similar shapes of the residuals and dark sky suggest that the subtraction of foregrounds has been incomplete and that the plotted values are upper limits. The thick solid line gives the CIB spectrum from the re-analysis of the COBE/FIRAS residuals, initiated in Puget *et al.* (1996) and revisited in Guiderdoni *et al.* (1997). The solid hexagons show the Cosmic Optical Background (COB) obtained by summing up faint galaxy counts down to the Hubble Deep Field limit. Strictly speaking, this is only a lower limit of the actual COB, but the shallowing of the *U* and *B*-band counts suggests near-convergence at least at those wavelengths (Williams *et al.* 1996). The short dashes and long dashes give the prediction for no-evolution integrated up to redshift $z_{for} = 8$ in a cosmology with $h = 0.5$ and $\Omega_0 = 1$. The other curves are computed for the SCDM model with $h = 0.5$, $\Omega_0 = 1$, $\sigma_8 = 0.67$, for scenarios Q, A, and E plotted with the line codes of tab. 1. Scenarios Q and A are not sufficient to reproduce the CIB. This suggests the existence of an additional population of ULIGs taken into account in scenario E.

The prediction for the evolution of the comoving SFR density is very similar to the result given by Baugh *et al.* (1997), though their model involves a more accurate procedure to compute the merging history of haloes (Cole *et al.* 1994). As in our model, they choose a SFR proportional to the ratio of the cold gas content to the dynamical time. But galaxies within haloes can merge after spiralling to the centre of the haloes induced by dynamical friction. During the merging, all the available gas is quickly converted into stars. In spite of this explicit implementation of a kind of “burst” mode, starbursting does not seem to affect significantly the SFR history, and the evolution they predict does not reproduce the steep decline of the SFR density between $z = 1$ and 0. Probably the modelling of dynamical friction alone underestimates the true magnitude of the interaction and merging processes between galaxies in merging haloes.

4.2 The “burst” mode of star formation

We now wish to introduce another mode of star formation with $\beta = 10$. The SFR time scales are now much shorter. As a result, the evolution of the luminosity function differs from the evolution in scenario Q involving the “quiescent” mode of star formation. As shown in fig. 2, the luminosity function of the “quiescent” mode is built up by the accumulation of light coming from all galaxies, and its evolution reproduces the evolution of the mass distribution of collapsed haloes. On the contrary, the luminosity function of the “burst” mode reproduces the evolution in the formation of haloes. Each generation of halo formation is accompanied by a strong starburst which acts as a transient beacon. As a consequence, the evolutionary trends of the luminosity functions in the two modes strongly differ.

Since we know that the local universe is dominated by the “quiescent” mode, we now consider a mix of two broad types of populations, one with a “quiescent” star formation rate, the other proceeding in bursts. For the “burst” mode, we take an involved mass fraction increasing with redshift $f_{burst}(z) = f_{burst}(0)(1+z_{coll})^\gamma$, as suggested by the increasing fraction of blue objects showing tidal and merger features at larger z (Abraham *et al.* 1996). Such a dependence is also consistent with theoretical considerations on the merger rates of galaxy pairs in merged haloes (Carlberg 1990). We limit the scope of the present paper to this phenomenological modelling of $f_{burst}(z)$. This is clearly a point which should be refined in forthcoming studies. Noting that the frequency of galaxy pairs is $\propto (1+z)^\delta$ with δ between 2 and 6 at $\pm 1\sigma$ (Zepf and Koo 1989; Burkey *et al.* 1994; Carlberg *et al.* 1994), we choose here a high evolution rate $\gamma = 5$. Then $f_{burst}(0)$ is set to 0.04 in order to fit the SFR density at low z , resulting in an “all-burst” behaviour at $z_{coll} \geq 0.8$. This will be our scenario A. As it appears from fig. 9, this phenomenological description of the increasing importance of bursts reproduces the steep decline of the SFR density. The origin of this fast evolution has still to be elucidated by a more exhaustive modelling of all interaction processes in the semi-analytic codes which follow the merging history trees of haloes and galaxies. Fig. 9 also shows that the predicted cosmic SFR history has a high- z evolution closer to the one derived from photometric estimates of redshifts rather than that from Lyman-continuum drop-outs. For instance, one should note that at $z = 4$, the predicted SFR is ten times the lower limit derived from the Lyman-continuum drop-outs *without extinction*. As a consequence of the high SFR, the gas content strongly evolves between $z \sim 2$ and 0, as shown in fig. 10.

We can now compute the corresponding IR/submm emission by taking the conservative estimate of the average optical thickness and “slab” geometry as in the “quiescent” mode. As a result, this population of “mild starbursts” and “luminous UV/IR galaxies” (LIGs) have IR-to-blue luminosity ratios in the range $0.06 \leq L_{IR}/\lambda_B L_B \leq 4$ which is characteristic of blue-band selected samples (Soifer *et al.* 1987), and should be fitted to the Canada-France Redshift Survey (selected in the observer-frame I_{AB} band, roughly corresponding to the *B* band at $z \sim 1$), and to high- z HDF galaxies. Galaxies at the peak of the SFR time-scale distribution ($t_* = 0.3$ Gyr) have $L_{IR}/M \simeq 6.3 L_{bol\odot}/M_\odot$. Nevertheless, their colours can still be very blue during the burst

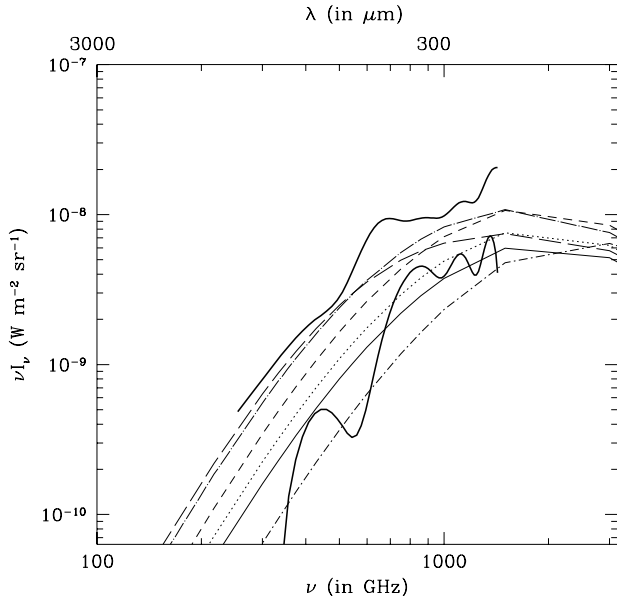


Figure 13. Predictions of the diffuse backgrounds in the FIR/submm (blow up), compared to the acceptable range of the CIB at $\pm 1\sigma$ per point (Guiderdoni *et al.* 1997). Scenarios Q, A, B, C, D, and E are plotted with line codes of tab. 1. The predictions for the COB are similar to those in fig. 12.

($B - V = 0.1$ at 0.5 Gyr). The evolution of the comoving luminosity density in various UV/visible bands and at 60 μm is compared to observational estimates in fig. 11. The local energy budget and its evolution from $z = 0$ to 1 seem to be fairly reproduced. The difference between the fits of the comoving SFR and luminosity densities (fig. 9 and 11) originates in the presence of dust absorption. The local UV flux is correctly fitted in fig. 11, while the local SFR in fig. 9 is about twice the value deduced from the local UV flux *under the assumption of no extinction*.

By integrating the contribution of sources along the line of sight, we can predict the corresponding diffuse backgrounds. While the results for both scenarios fairly reproduce the COB, as shown in fig. 12, scenario A does not do much better than scenario Q to reproduce the CIB. Their predictions are clearly barely compatible with the acceptable $\pm 1\sigma$ range recalled in fig. 13. The mean amplitude of the CIB is twice the prediction, despite our high choice of γ . Consequently, we can strongly suspect the existence of a population of galaxies which are more heavily extinguished.

4.3 A heavily-extinguished component

The above-mentioned CIB computed with scenario A seems to be something like a conservative estimate of the minimum IR/submm background due to typical CFRS and HDF galaxies. We now wish to assess how much star formation might be hidden by dust shrouds and introduce an additional population of heavily-extinguished bursts, which are similar to “ultra-luminous IR galaxies”, or ULIGs (Sanders and Mirabel 1996; Clements *et al.* 1996a). We maximize their IR luminosity by assuming that all the energy avail-

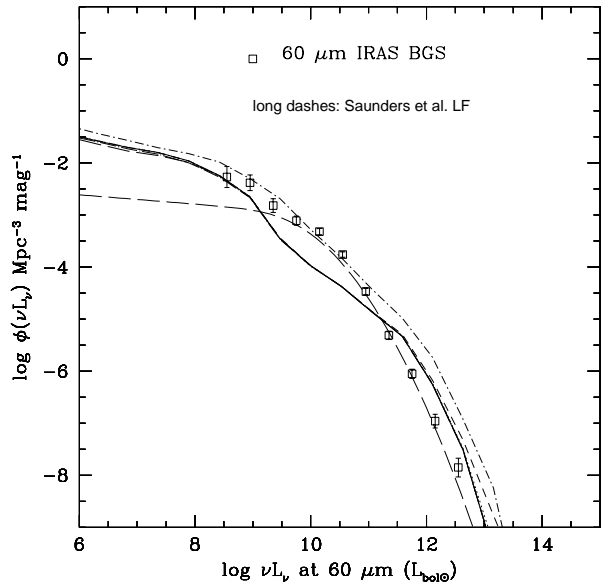


Figure 14. Predicted 60 μm luminosity functions at $z = 0$ for the SCDM model with $h = 0.5$, $\Omega_0 = 1$ and $\sigma_8 = 0.67$. Scenarios Q, A, B, C, D, and E are plotted with line codes of tab. 1. At $z = 0$, scenarios A, B, C, D, E give almost similar results since the “burst” mode only involves 4 % of the mass. Scenario Q gives a slightly higher luminosity function since more gas is left to fuel star formation at $z = 0$. Squares: observational luminosity function for the *IRAS* Bright Galaxy Sample (Soifer and Neugebauer 1991). Thick long dashes: observational luminosity function from a compilation of various samples (Saunders *et al.* 1990).

able from stellar nucleosynthesis ($0.007xMc^2$) is radiated in a heavily-extinguished medium, yielding a total IR luminosity $L_{\text{IR}}/M \simeq 42.5(x/0.40)(t_*/1\text{Gyr})^{-1} L_{\text{bol}\odot}/M_\odot$, provided the lifetimes of stars are smaller than the duration t_* of the burst. We take $\langle x \rangle = 0.40$ for stars with masses larger than $\sim 5M_\odot$ (Schaller *et al.* 1992), and get luminosities which are a factor ~ 20 larger than those of our mild-starburst/LIG mode. As a consequence of this simple model, the starburst only radiates in the IR/submm, and only dark remnants are left when it stops, without the slow evolution of low-mass stars. We distribute this population of ULIGs in two ways: i) A constant mass fraction of 5 % (scenario B) or 15 % (scenario D) at all z_{coll} , mimicking a scenario of continuous bulge formation as the end-product of interaction and merging. ii) 90 % of all galaxies forming at high $z_{\text{coll}} \geq 3.5$ undergo a heavily-extinguished burst, mimicking a strong episode of bulge formation. These scenarios are now able to fit both the COB and CIB. Scenarios B and D seem more appropriate to reproducing the CIB at 300 μm while scenario C, with high- z ULIGs, has a stronger contribution at larger wavelengths. Of course, these last three cases are only illustrative, and a combination of these solutions would also fit the CIB. For instance, we introduce an ad hoc scenario E with a fraction of ULIGs increasing as $1 - \exp -0.02(1 + z_{\text{coll}})^2$. Such a dependence can be obtained if the fraction of ULIGs depends on the mean surface density and optical thickness of disks which roughly scale as

$(1 + z_{coll})^2$ in our modelling. As shown by fig. 12 and 13, scenario E nicely reproduces the COB and CIB, and could be considered as our “best fit”.

It is clear from fig. 11 that none of the optical data reflects the large differences between these scenarios, although the fraction of light in the IR varies widely at high z . In scenario A, the IR/UV ratio decreases with increasing z because of the decreasing metallicity of galaxies. In scenario B and D, this effect is cancelled because the ULIG bursts are assumed to be optically-thick, with a top-heavy IMF, and the IR/UV ratio at $z = 4$ is similar to that at $z = 0$. In scenario C and E, the IR/UV ratio strongly increases with z and is ~ 100 times higher than for model B at $z = 4$. One should note that at this redshift, scenario C and E are roughly consistent with the lower limits of the UV-luminosity density derived from Lyman-continuum drop-outs, but with ten times as much SFR as directly derived if extinction is not taken into account. In these scenarios, galaxy formation at high z is an almost completely-obscured process.

We emphasize that the family of scenarios summarized in tab. 1 is introduced within the same SCDM model. The dissipative and non-dissipative collapses are unchanged, and the characteristic time scale for the conversion of gas into stars is always proportional to the local dynamical time, which is the most natural time scale. Given that, we only change the “fuzzy” astrophysics introduced with the efficiency parameter β . It seems reasonable to *assume* that the efficiency of star formation is typically an order of magnitude greater for interacting galaxies (the “burst” mode) than for isolated galaxies (the “quiescent” mode), resulting in a β parameter an order of magnitude lower. While this assumption has yet to be put on firmer grounds, its effect on the global SFR and gas densities is very strong. As a second step, changes in the IMF and extinction can modify the optical and IR/submm energy budget.

5 PREDICTIONS IN THE FIR AND SUBMM

5.1 The FIR luminosity function

Fig. 14 gives predictions for the $z = 0$ luminosity function at $60 \mu\text{m}$ compared with the observational determinations drawn from the *IRAS* Bright Galaxy Sample (Soifer and Neugebauer 1991) and from a compilation of various *IRAS* samples (Saunders *et al.* 1990). The difference of the two observational luminosity functions at the faint end illustrates the uncertainties. The agreement of the predictions with the data is fair. It is not surprising that scenario Q seems to give a better fit, since most galaxies of the BGS are spirals, mild starbursts and LIGs. All the scenarios involving the burst mode (A to E) give similar results at $z = 0$ since the fraction of mass involved in starbursts is low (4 %). Burst scenarios with shorter SFR time scales in the past consumed more gas than scenario Q and less fuel is now left for star formation.

It has been recalled in Sec. 2.6 that this kind of semi-analytic models predicts too many low-luminosity galaxies in the optical bands at $z = 0$, with respect to the observational field luminosity functions (see the references quoted in Sec. 2.6). As a consequence, the optical luminosity functions are too steep and can be reconciled with the observations by

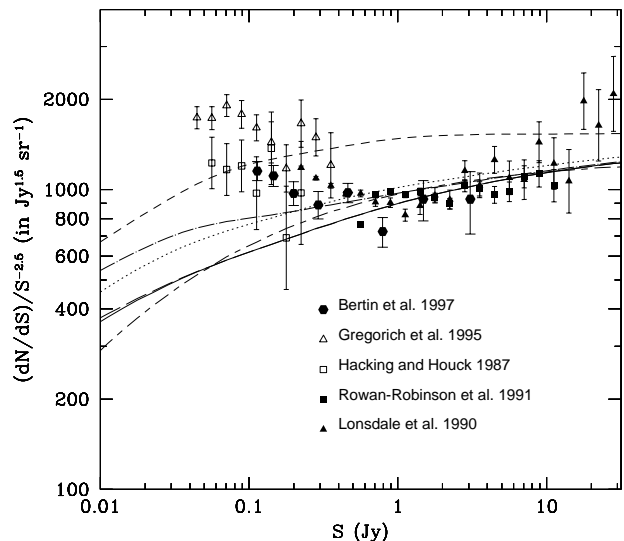


Figure 15. Predictions for differential galaxy counts (normalised to Euclidean counts) at $60 \mu\text{m}$. Data is shown for *IRAS* counts at $60 \mu\text{m}$. Solid triangles: Faint Source Survey (Lonsdale *et al.* 1990). Solid squares: QMW survey (Rowan-Robinson *et al.* 1991b). Solid hexagons: revisited counts in the Very Faint Source Survey (Bertin *et al.* 1997). Open squares: North Ecliptic Pole Region (Hacking and Houck 1987). These latter counts might be affected by the presence of a super-cluster. The counts by Gregorich *et al.* (1995), which are plotted with open triangles, are probably contaminated by cirrus. The no-evolution model (for a cosmology with $h = 0.5$, $\Omega_0 = 1$) is shown with short dashes and long dashes. Scenarios A, B, C, D, E are plotted with line codes of tab. 1. Scenario D has too many local ULIGs and should be rejected. Scenario E with an increasing fraction of ULIGs almost reproduces the flat behaviour of the counts.

invoking subtle selection effects based on surface brightness. Our model also predicts too many low-luminosity galaxies in the IR, while the discrepancy is somewhat lower than in the blue. The slope is $\phi(L_{IR})dL_{IR} \propto L_{IR}^{-1.25}dL_{IR}$. The normalisation at the bright end can be improved by a slight decrease (a few tenth dex) of the baryonic density Ω_{bar} , or a slight increase of the baryonic mass-to-luminosity ratios, through the normalisation of the “dark mass” in the IMF. We do not attempt to apply this kind of fine tuning.

5.2 Faint galaxy counts

We hereafter explore the faint counts predicted by using the scenarios proposed in tab. 1. Fig. 15 gives the predictions for the *IRAS* $60 \mu\text{m}$ differential counts normalised to the Euclidean slope. Observational counts from the QMW survey (Rowan-Robinson *et al.* 1991b), the Faint Source Survey (Lonsdale *et al.* 1990), the Very Faint Source Survey (Bertin *et al.* 1997), and the North Ecliptic Pole Region (Hacking and Houck 1987) are superimposed to the predictions. The latter survey might be partly affected by a large-scale structure at $z = 0.088$ (Ashby *et al.* 1996). As shown by Bertin *et al.* (1997), the counts by Gregorich *et al.* (1995) are contam-

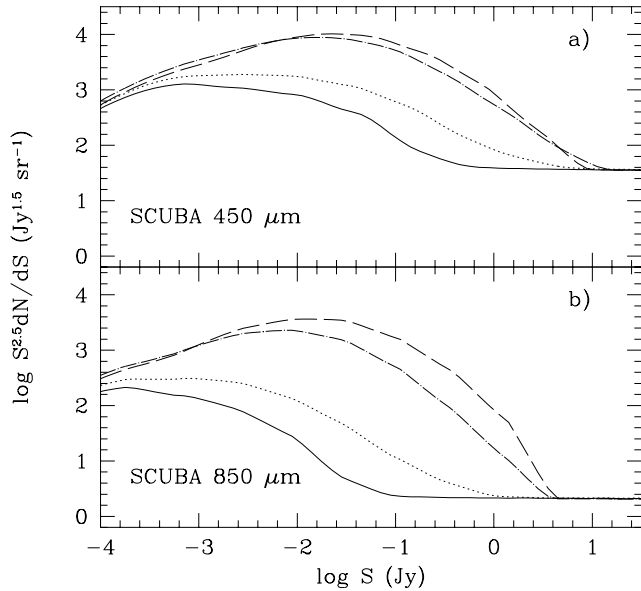


Figure 16. Predictions for differential galaxy counts (normalised to Euclidean counts) at 450 and 850 μm for observations with SCUBA. In contrast with counts at wavelengths smaller than 100 μm , the submm counts are very sensitive to the details of the high- z evolution, because of the shift of the 100 μm bump into the observing bands. Scenarios A, B, C and E are plotted with line codes of tab. 1.

inated by cirrus. The theoretical curves are *not* renormalised to the bright end of the observed counts. The scenarios involving an increasing fraction of the “burst” mode predict more galaxies than the no-evolution curve. Scenario D with 15 % of ULIGs is rejected by the data. All the other scenarios have a moderate local fraction of ULIGs and are in agreement with the faint counts. Scenario E with an increasing fraction of ULIGs gives an almost flat curve which is reminiscent of the observational trend. Nevertheless, the rise of the counts below 0.1 Jy, if it is real, is not reproduced. However, our scenarios predict a correct amount of fluctuation and there is not much space for stronger evolution. More specifically, the counts predict a 60 μm background fluctuation per beam in the Very Faint Source Survey (after removal of $\geq 4\sigma_{\text{tot}} = 120$ mJy sources) at the level of 14.1 mJy (A), 16.0 mJy (B), 14.3 mJy (C) and 17.0 mJy (E), while the measured 68 % quantile is 30.1 ± 1.2 mJy (Bertin *et al.* 1997). With a 25 mJy *rms* instrumental noise and 6.5 mJy *rms* cirrus fluctuations (Gautier *et al.* 1992), there is still space for a $15.4^{+2.2}_{-2.5}$ mJy fluctuation due to sources, in good agreement with our estimates. Moreover, if the cirrus fluctuations are non-gaussian, the *rms* value strongly overestimates the 68 % quantile and can tolerate $16.8^{+2.0}_{-2.3}$ mJy for source fluctuation.

Fig. 16 and 17 give the predictions for various wavelengths from 15 μm to 1.4 mm which correspond to current and forthcoming instruments. The *IRAS* 60 μm counts are recalled in one of the panels, as well as the ISO-HDF 15 μm deep counts (Oliver *et al.* 1997). Only scenarios A and E are plotted. Clearly there are three regimes: (i) Nearby

galaxies are in the Euclidean zone, giving a count slope $N(> S) \propto S^{-3/2}$. The value of the bright-end normalisation at submm wavelengths depends on the choice of the emissivity index m . Since the count rates are very low, it is likely that we shall have to wait for the all-sky survey of *PLANCK* in order to fix the counts at the bright end. (ii) At short wavelengths, the curvature effect and the positive “k-correction” produce the bend of the faint counts; (iii) In the submm/mm range, the negative “k-correction” produces a bump in the faint counts, which reflects the passage of the 100 μm emission bump into the observing bands.

It appears from fig. 17 that the ISO-HDF counts suggest evolution, but that the predictions are not strongly sensitive to the details of the evolutionary scenario. Guiderdoni *et al.* (1997) have emphasized the relative degeneracy of the predictions at wavelengths shorter than 100 μm , including the *IRAS* 60 μm and the *ISO* 15 μm counts, and the strong sensitivity of the submm counts to the details of galaxy evolution, which is already apparent for *ISO* observations at 175 μm . Tab. 2 and 3 gather the count predictions for the various scenarios of tab. 1, and two typical sensitivity levels: 100 mJy which will be reached for point sources by the *PLANCK* all-sky survey, and which is comparable to the 0.22 Jy level of the *IRAS* 60 μm Faint Source Catalogue; and 10 mJy which can be reached by a deep pencil-beam survey with SCUBA and *FIRST*. The number counts at 100 mJy and 10 mJy are very sensitive to evolution and can differ by an order of magnitude at 350 μm , and more than two orders of magnitude at 850 μm . This explains the discrepancy of the predictions in the literature so far published. Hivon *et al.* (1997) will come back to the detection of submm sources and of the fluctuations they induce. As a conclusion of these predictions, while the *IRAS* data do not yield tight constraints on the evolution of galaxies at $z \geq 0.2$, the forthcoming deep survey with *ISO* at 175 μm and with SCUBA in the atmospheric windows at 450 and 850 μm (for which the array is matched to the instrument optics) will quickly help discriminate between the various scenarios, in the expectation of *PLANCK* and *FIRST*.

5.3 Redshift distributions

Fig. 18 shows the prediction for the redshift distribution corresponding to the spectroscopic follow-up of two *IRAS* samples: the North Ecliptic Pole Region observed by Ashby *et al.* (1996) with 60 μm fluxes $60 \leq S_{60} \leq 150$ mJy, and the sample of Clements *et al.* (1996a) for galaxies of the Faint Source Catalogue with $S_{60} \geq 300$ mJy which are “IR loud” (IR-to-blue ratios larger than 10). The data of the NEPR are almost complete and can be directly compared to our predictions. Nevertheless, the first two bins are probably affected by a super-cluster at $z = 0.088$. The redshifts of the “IR-loud” FSC sample have been taken by the authors in order to extract a subsample of ULIGs and not for a complete redshift survey. The histogram given for the galaxies which are not ULIGs (144 sources) has been roughly rescaled to take into account the number of sources not quoted in their Appendix because they already have redshifts in the literature. The shaded histogram shows their 91 ULIGs. Then the histogram is renormalised in order to peak at the same relative level as the NEPR. The sample has only a 60 % completeness. In general, the scenarios seem to predict more

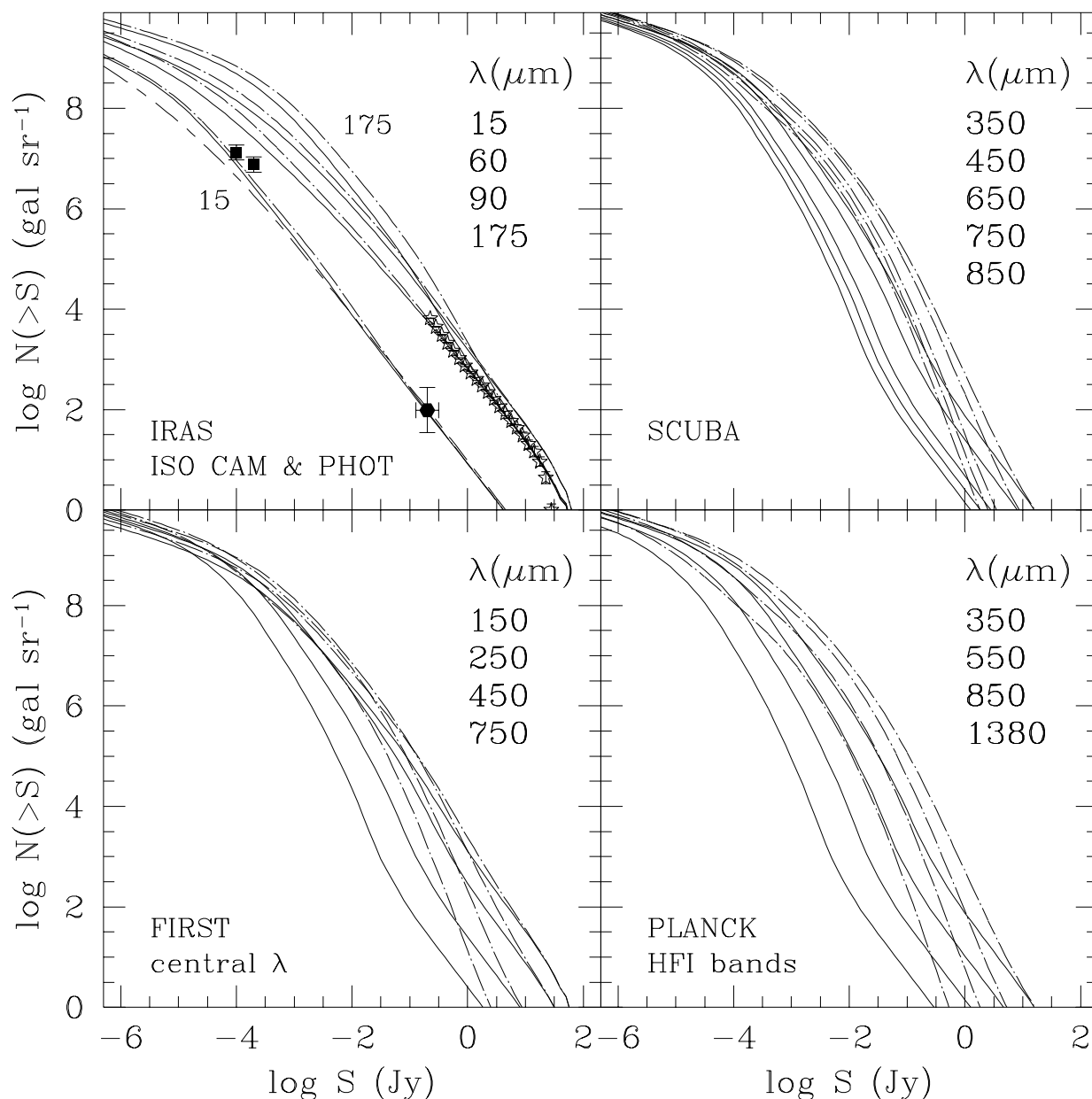


Figure 17. Predictions for number counts at various wavelengths for operating and forthcoming observing facilities and experiments: ISOCAM and ISOPHOT on-board *ISO*, SCUBA, *FIRST*, and *PLANCK* High Frequency Instrument. Some of the curves are redundant. The curves correspond to the wavelengths from top to bottom, except in the *IRAS/ISO* Panel where it is from bottom to top. Note that the 15 μm curve only takes into account dust emission (without the stellar component), and the observer-frame fluxes should be considered as lower values beyond $z \sim 1$. The no-evolution prediction at 15 μm (for $h = 0.5$ and $\Omega_0 = 1$) is plotted with short dashes and long dashes. Open stars: *IRAS* at 60 μm (Lonsdale *et al.* 1990). Solid hexagon: *IRAS* at 12 μm (Rush *et al.* 1993). Solid squares: *ISO*-HDF counts at 15 μm (Oliver *et al.* 1997). Scenarios A and E are plotted with line codes as in tab. 1.

galaxies at high z than in the NEPR sample. The “IR-loud” FSC sample plotted here suffers from problems of overall normalisation and incompleteness, but it signals the presence of galaxies at $z \geq 0.2$. The difference between the redshift distributions for scenarios E and A gives the fraction of ULIGs in scenario E (there are no ULIGs in scenario A). The distribution of ULIGs with z seems to be much flatter

than the observed peak in the “IR-loud” FSC sample. However, it is difficult to assess the level of discrepancy with a 60 % the incompleteness. Clearly the redshift follow-up of deep IR-selected samples is still an on-going project, and it will bring crucial information on the nature of the sources.

Fig. 19 shows predictions for the redshift distributions at 60, 200, 350, and 550 μm , corresponding to various flux

Table 2. Predictions of galaxy counts in *PLANCK* HFI bands at the 100 mJy level (log number of sources sr⁻¹).

Name	350 μ m	550 μ m	850 μ m	1380 μ m
Q	3.97	3.06	2.15	1.18
A	3.93	2.73	1.67	0.71
B	4.41	3.48	2.23	0.83
C	4.95	4.88	4.39	3.15
D	5.04	4.34	3.33	1.77
E	5.08	4.57	3.83	2.39

Table 3. Predictions of galaxy counts in SCUBA and *FIRST* bands at the 10 mJy level (log number of sources sr⁻¹).

Name	350 μ m	450 μ m	650 μ m	750 μ m	850 μ m
Q	5.66	5.23	4.41	4.09	3.80
A	5.98	5.63	4.73	4.40	3.98
B	6.27	5.99	5.34	5.07	4.75
C	6.80	6.81	6.64	6.52	6.37
D	6.66	6.47	6.01	5.80	5.55
E	6.84	6.75	6.45	6.29	6.09

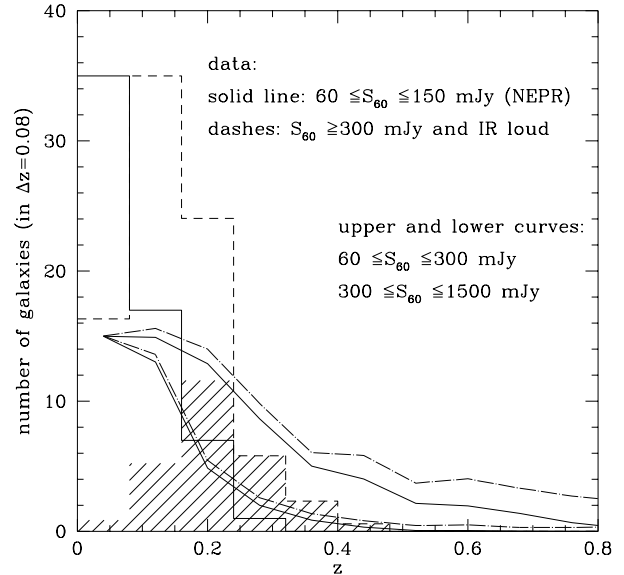
depths. Scenarios A and E (as well as B, C, and D not plotted here) give different predictions at $z \geq 1$. For scenario A, the redshift distributions at the 10 mJy flux level peak at $z \sim 1$, with a high- z tail encompassing 90 % of the sources at $z \sim 2.5$ to 3. Scenario E has galaxies at still higher z . In contrast with the *IRAS* samples at 60 μ m which, at the 100 mJy flux level, only probe the universe at $z \sim 0.2$, the future spectroscopic follow-up of submm observations at the 10 mJy level should be able to explore the IR/submm evolution of galaxies at $z \geq 1$. Finally, fig. 20 shows the contribution of sources fainter than S to the background value at 60, 200 and 550 μ m. The 10 mJy level which will be reachable by the forthcoming submm observations will allow the surveys to begin “breaking” the CIB into discrete units.

6 DISCUSSION AND CONCLUSIONS

We have used a simple semi-analytic model of galaxy formation to derive the IR/submm statistical properties of galaxies: luminosity function, faint galaxy counts, redshift distributions, and the diffuse background. The model shares many common features with previous semi-analytic works focussing upon the optical properties of galaxies: (i) the collapse of the perturbations is described by the classical top-hat model under the assumptions of homogeneity and sphericity; in this simple version, we used the peaks formalism to compute the formation rate of haloes. (ii) the dissipative cooling and collapse is introduced, with the usual “overcooling” problem which can be partly suppressed by introducing feedback due to overall re-ionization and galactic winds triggered by SNe. (iii) star formation is proportional to the ratio of the gas content to the dynamical time scale of the galaxies; and (iv) stellar evolution is explicitly implemented.

In order to make specific predictions for the IR/submm wavelength range, this model includes the following assumptions:

- (i) An average optical depth of the disks is implemented

**Figure 18.** Predicted redshift distribution of the North Ecliptic Pole Region observed by Ashby *et al.* 1996. The observed galaxies have 60 μ m fluxes in the range $60 \leq S_{60} \leq 150$ mJy. The first two bins might be affected by a super-cluster. The sample of Clements *et al.* (1996a) is also plotted for sake of illustration. The reader is referred to this paper for the description of the selection criteria. Roughly, the galaxies have $S_{60} \geq 300$ mJy and are “IR loud” (IR-to-blue ratio larger than 10). See text for the details. The shaded histogram show the ULIGs of this sample. Scenarios A and E are plotted with line codes of tab. 1. Their normalisation is relative.

and scales as the relative gas content and gas metallicity (estimated through the assumption of Instant Recycling Approximation); no evolution of the dust composition is considered; the variation of the extinction curve with metallicity is based on an interpolation of the Milky Way and the Magellanic Clouds which gives an extinction proportional to $Z^{1.6}$;

- (ii) A simple “slab” geometry is assumed where dust and stars are mixed with equal height scales;

- (iii) Finally, the dust emission spectrum scales with the bolometric IR luminosity, following the observational relationship of *IRAS* colours with luminosities. Such a dependence is obtained by changing the abundance of three components: PAH, very small grains and big grains (and the temperature of the big grains).

We introduced two modes of star formation. In the “quiescent” mode, the distribution of the characteristic time scales t_* for star formation peaks at 3 Gyr, and ranges from 0.3 to 30 Gyr. In the “burst mode”, the distribution of t_* peaks at 0.30 Gyr, and ranges from 0.03 to 3 Gyr. The “quiescent” mode is unable to reproduce the rapid evolution of the cosmic SFR and gas densities. The steep decline of the SFR and gas content since $z = 2$ can be accommodated by assuming an increasing fraction of mass involved in the “burst” mode. Since one knows that the fraction of peculiar objects with signs of interaction/merging increases with

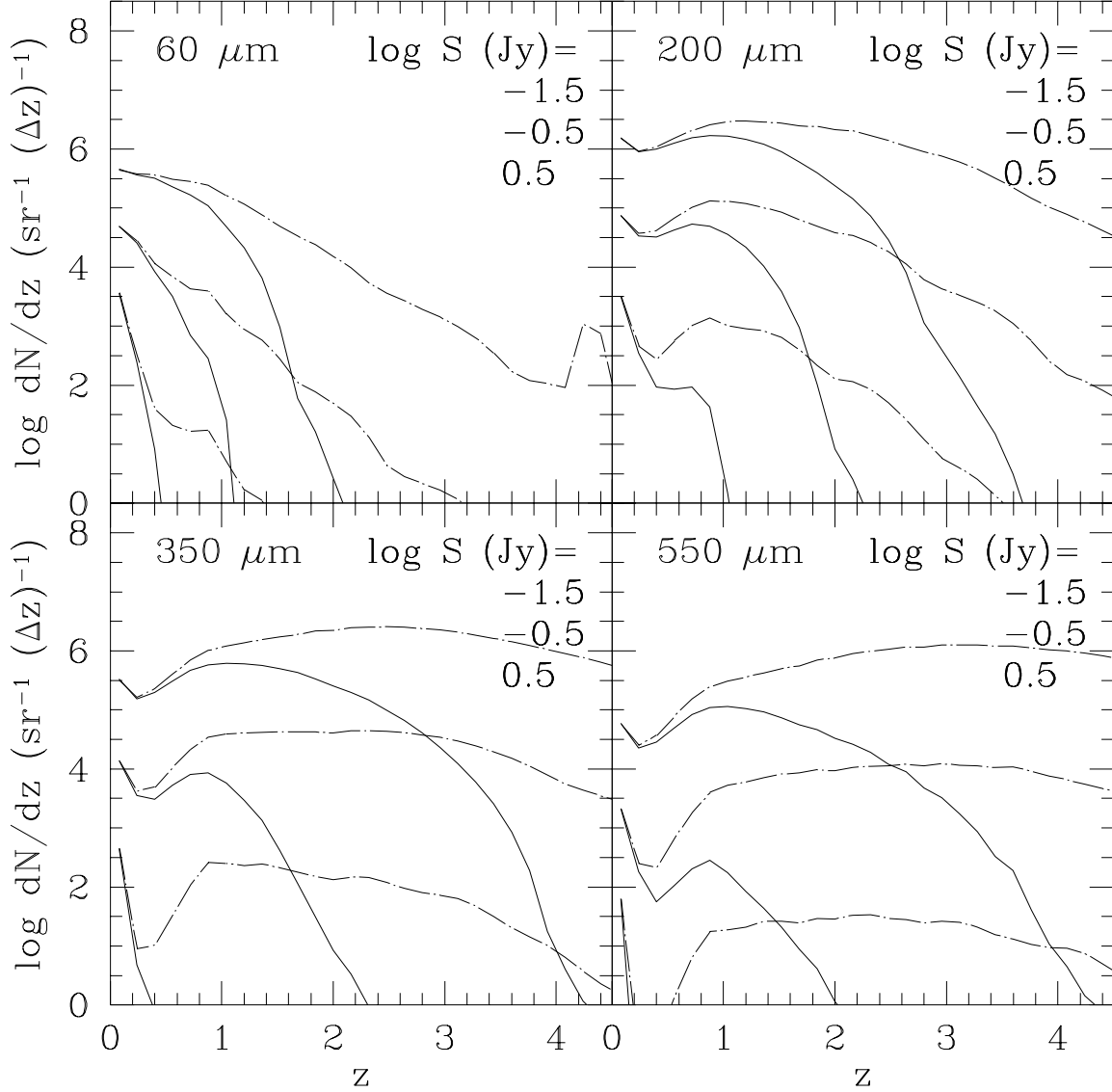


Figure 19. Predictions for redshift distributions at four wavelengths, and in different flux ranges. The flux bin widths are $\Delta \log S = 1$, and the central flux values ($\log S$ in Jy) are shown in each figure (from top to bottom). Scenarios A and E are plotted with line codes of tab. 1.

the depth of the survey, we suspect that the bursting behaviour of the CFRS and HDF galaxies is due to interactions and we introduce a phenomenological z dependence fitting the evolution of the pair rates. Since LIGs and ULIGs are respectively interacting and merging systems, it is reasonable to estimate that, reciprocally, CFRS and HDF galaxies with peculiar morphologies should emit in the IR. For these “mild starbursts” and “luminous IR/UV galaxies”, we assume a conservative range of IR-to-blue luminosity ratios $0.06 \leq L_{IR}/\lambda_B L_B \leq 4$ computed from our standard assumptions on average optical thickness and geometry. Finally, in order to reproduce the bright end of IR galaxies with $L_{IR}/\lambda_B L_B \geq 10$, we also introduced a population of

heavily-extinguished galaxies with massive star formation, similar to ULIGs.

With these ingredients, we designed a family of evolutionary scenarios which fit the local overall energy budget and its evolution to $z \sim 1$. These scenarios also fit the COB estimate computed from faint galaxy counts, and are consistent with the observational range for the CIB. So we feel confident that we roughly reproduce the local energy budget as well as a plausible range for the integrated budget along the line of sight. The scenarios predict UV and IR emissions strongly differing at high z . With the same SFR history, different UV fluxes can be obtained with different extinctions and IMF. In some of the scenarios, the UV fluxes

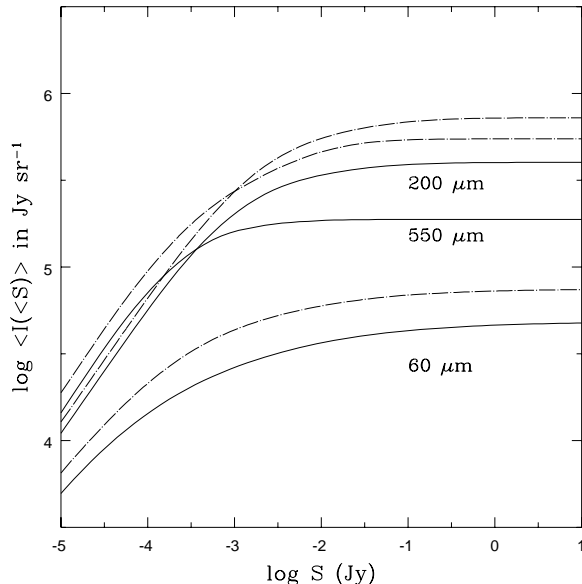


Figure 20. Contribution of sources fainter than S to the background value at 60, 200 and 550 μm . Scenarios A and E are plotted with line codes of tab. 1.

at $z = 4$ fit the current measurements (or lower values) of Madau *et al.* (1996), but with ten times more SFR than deduced *under the assumption of no extinction*. Such a factor 10, which includes the contribution of heavily-extinguished ULIGs, is much larger than the factor 3 corresponding to the correction for extinction derived by Pettini *et al.* (1997) for the HDF galaxies with Lyman-continuum drop-outs. This quantifies the strong warning that the deduction of the SFR density from UV fluxes misses the optically-dark side of galaxy formation.

This family of scenarios was obtained within the context of the same cosmological model, with similar prescriptions for dissipative and non-dissipative collapses, star formation and feedback. The changes only affect the efficiency of star formation in a dynamical time scale (the β parameter), the IMF (Salpeter or only massive stars), and the extinction (average extinction with “slab” geometry, or strong, “screen”-like extinction). We saw the extreme sensitivity of the predictions to the parameter choice for this poorly constrained astrophysics.

The scenarios are consistent with *IRAS* data. They give similar predictions for the *IRAS* 60 μm luminosity function and faint counts, provided the local fraction of ULIGs is lower than a few %. They are in rough agreement with the redshift surveys of *IRAS* samples, in spite of some uncertainty in the data. By construction, the IR spectra also fit the correlation of IR colours with total IR luminosity in the Bright Galaxy Sample. The selected scenarios are consistent with the $\pm 1\sigma$ range for the observed CIB and they are used to “disentangle” the background into faint galaxy counts. This CIB is the first “post-*IRAS*” observation which helps constraining the high- z evolution of galaxies in the IR/submm and the energy budget integrated along the line-of-sight, before *ISO* results. In contrast with the counts at

FIR wavelengths which are rather degenerate, the submm counts are very sensitive to the details of the evolutionary scenarios. Thus our study illustrates the importance of the submm range to constrain the evolution of the energy budget of galaxies. As emphasized by Guiderdoni *et al.* (1997), our understanding of the formation and evolution of galaxies is so far entirely based on surveys in the UV/visible window. We are missing the part of star/galaxy formation hidden by dust. We need to open a second window in the IR/submm, which is being explored by *ISO* and SCUBA, and will be extensively studied by forthcoming telescopes and satellites such as *SIRTF*, *SOFIA*, *FIRST* and *PLANCK*.

There are clearly many approximations and shortcomings in our approach, which could be listed as a research programme for forthcoming papers. (i) We need to implement the astrophysical processes in a code which explicitly follows the merging history trees of haloes and galaxies. This code would have to include the various aspects of interaction between galaxies, and to explain why the interaction rate strongly declined since $z = 1$. It would also have to include the effect of interactions on the SFR. (ii) The modelling of the IR emission could take into account the evolution of dust properties with chemical abundances, as well as more sophisticated transfer. (iii) The global energy budget of galaxies has to be addressed by fitting the faint galaxy counts in the UV/visible and K , as well as the forthcoming NIR counts from *ISO*, in particular at 15 μm . First results are already given here, and suggest an amount of evolution which is consistent with our predictions. (iv) The strong evolution of the comoving SFR density has consequences on the gas and heavy element abundances. The heavy elements made by the high SFRs are to be found in the stars, the cold gas, or the hot gas of the intergalactic medium. If the SFR turned out to be much higher than determined, for instance, by Madau *et al.* (1996), a significant fraction of the heavy elements should be present in the IGM. The amount of elements synthesised in bursts would still be higher if the IMF is top-heavy, as in the simple model of ULIGs which is used here. According to Mushotzky and Loewenstein (1997), the absence of evolution of the iron content of clusters at $z \sim 0.3$ is a first evidence that the global metal production is 2–5 times higher than inferred from the UV drop-out technique.

Despite the limitations listed above, this paper provides the first predictions of the IR luminosity function, IR/submm galaxy counts, redshift distributions, and diffuse background, obtained from a semi-analytic model of galaxy formation and evolution which takes into account the main physical processes from the collapse of the density fluctuations to the absorption of UV and visible star light by dust and the re-emission in the IR/submm range. The predictions of this new model are consistent with the dynamical process of continuous galaxy formation predicted by the hierarchical growth of structures in a SCDM universe, and represent a significant progress with respect to previous phenomenological models designed to make predictions in the IR/submm.

Tables giving the faint counts and redshift distributions at various wavelengths between 15 μm and 2 mm are available by anonymous ftp at **ftp.iap.fr** in the directory /pub/from_users/guider/fir, and on the Web node of the Institut d’Astrophysique de Paris at **http://www.iap.fr/users/guider/fir.html**.

Acknowledgements. We are pleased to thank Stéphane Charlot, Dave Clements, François-Xavier Désert, David Elbaz, Michael Fall, Karl Glazebrook and Jean-Loup Puget for their comments and suggestions.

REFERENCES

- Abraham, R.G., Tanvir, N.R., Santiago, B.X., Ellis, R.S., Glazebrook, K., van den Bergh, S., 1996, MNRAS, 279, L47
- Andreani, P., Franceschini, A. 1992, A & A, 260, 89
- Andreani, P., Franceschini, A., 1996, MNRAS, 283, 85
- Ashby, M.L.N., Hacking, P.B., Houck, J.R., Soifer, B.T., Weisstein, E.W., 1996, ApJ, 456, 428
- Bardeen, J.M., Bond, J.R., Kaiser, N., Szalay, A.S. 1986, ApJ, 304, 15
- Barnes, J., Efstathiou, G. 1987, ApJ, 319, 575
- Baugh, C.M., Cole, S., Frenk, C.S., 1996a, MNRAS, 283, L15
- Baugh, C.M., Cole, S., Frenk, C.S., 1996b, MNRAS, 283, 1361
- Baugh, C.M., Cole, S., Frenk, C.S., Lacey, C.G., 1997, astro-ph/9703111
- Beichman, C.A., Helou, G. 1991, ApJL, 370, L1
- Bertin, E., Dennefeld, M., Moshir, M. 1997, A&A, 323, 685
- Blain, A.W., Longair, M.S., 1993a, MNRAS, 264, 509
- Blain, A.W., Longair, M.S., 1993b, MNRAS, 265, L21
- Blanchard, A., Valls-Gabaud, D., Mamon, G., 1992, A&A, 264, 365
- Bond, J.R., Cole, S., Efstathiou, G., Kaiser, N., 1991, ApJ, 379, 440
- Bond, J.R., 1988, in *The Early Universe*, Unruh & Semanoff (eds.), p. 322
- Bower, R.G., 1991, MNRAS, 248, 332
- Briggs, F.H., Rao, S., 1993, ApJ 417, 494
- Burkey, J.M., Keel, W.C., Windhorst, R.A., Franklin, B.E., 1994, ApJ, 429, L13
- Carlberg, R.G., 1990, ApJ, 359, L1
- Carlberg, R.G., Pritchet, C.J., Infante, L., 1994, ApJ, 435, 540
- Carico, D.P., Keene, J., Soifer, B.T., Neugebauer, G., 1992, PASP, 104, 1086
- Chini, R., Kreysa, E., Krügel, E., Mezger, P.G., 1986, A&A, 166, L8
- Charbonnel, C., Meynet, G., Maeder, A., Schaerer, D., 1996, A&ASS, 115, 339
- Chini, R., Krügel, E., 1993, A&A, 279, 385
- Clements, D.L., Andreani, P., Chase, S.T., 1993, MNRAS, 261, 299
- Clements, D.L., Sutherland, W.J., Saunders, W., Efstathiou, G.P., McMahon R.G., Maddox, S., Rowan-Robinson, M., 1996a, MNRAS, 279, 459
- Clements, D.L., Sutherland, W.J., McMahon R.G., Saunders, W., 1996b, MNRAS, 279, 477
- Cole, S., 1991, ApJ, 367, 45
- Cole, S., Aragón-Salamanca, A., Frenk, C.S., Navarro, J.F., Zepf, S.E. 1994, MNRAS, 271, 781
- Connolly, A.J., Szalay, A.S., Dickinson, M., SubbaRao, M.U., Brunner, R.J., 1997, astro-ph/9706255
- Cowie, L.L., Songaila, A., Hu, E.M., Cohen, J.D., 1996, AJ, 112, 839
- Dekel, A., Silk, J., 1986, ApJ, 303, 39
- Désert, F.X., Boulanger, F., Puget, J.L. 1990, A&A, 237, 215
- Disney, M., Davies, J., Philipps, S., 1989, MNRAS, 239, 939
- Draine, B.T., Lee, H.M., 1984, ApJ, 285, 89
- Dwek, E., Városi, F., 1996, in *Unveiling the Cosmic Infrared Background*, E. Dwek (ed), AIP Conference Proceedings 348
- Eales, S.A., Wynn-Williams, C.G., Duncan, W.D., 1989, ApJ, 339, 859
- Eales, S.A., Edmunds, M.G., 1996a, MNRAS, 280, 1167
- Eales, S.A., Edmunds, M.G., 1996b, astro-ph/9609120
- Efstathiou, G., Rees, M.J. 1988, MNRAS, 230, 5P
- Efstathiou, G., Frenk, C.S., White, S.D.M., Davis, M. 1988, MNRAS, 235, 715
- Efstathiou, G., 1992, MNRAS, 256, 43P
- Eisenhardt, P., Armus, L., Hogg, D.W., Soifer, B.T., Neugebauer, G., Werner, M.W., 1996, ApJ, 461, 72
- Ellis, R.S., Colless, M., Broadhurst, T.J., Heyl, J.S., Glazebrook, K., 1996, MNRAS, 280, 235
- Evrard, A.E., 1989, ApJ, 341, 26
- Fall, S.M., Efstathiou, G., 1980, MNRAS, 193, 189
- Fall, S.M., Charlot, S., Pei, Y.C., 1996, ApJ, 464, L43
- Franceschini, A., Toffolatti, L., Mazzei, P., Danese, L., & De Zotti, G., 1991, ApJSS, 89, 285
- Franceschini, A., Mazzei, P., De Zotti, G., Danese, L. 1994, ApJ, 427, 140
- Franceschini, A., Andreani, P. 1995, ApJ, 440, L5
- Gautier, T. N., III, Boulanger, F., Perault, M., Puget, J. L., 1992, AJ, 103, 1313
- Griffiths, R.F., *et al.*, 1994, ApJ, 437, 67
- Guiderdoni, B., 1987, A&A, 172, 27
- Guiderdoni, B., Rocca-Volmerange, B. 1987, A&A, 186, 1
- Guiderdoni, B., Rocca-Volmerange, B. 1988, A&ASS, 74, 185
- Guiderdoni, B., Hivon, E., Bouchet, F.R., Maffei, B., & Gispert, R. 1996, in *Unveiling the Cosmic Infrared Background*, E. Dwek (ed), AIP Conference Proceedings 348
- Guiderdoni, B., Bouchet, F.R., Puget, J.L., Lagache, G., Hivon, E., 1997, *submitted*
- Hacking, P., Houck, J.R., 1987, ApJSS, 63, 311
- Hacking, P.B., Soifer, B.T. 1991, ApJL, 367, L49
- Haehnelt, M.G., Rees, M.J., 1993, MNRAS, 263, 168
- Hauser, M.G. 1995, in *Proceedings of the IAU Symp. n° 168, Examining the Big Bang and Diffuse Background Radiation*, The Hague, August 1994
- Helou, G., Soifer, B.T., Rowan-Robinson, M., 1985, ApJ, 298, L7
- Heyl, J.S., Cole, S., Frenk, C.S., Navarro, J.F., 1995, MNRAS, 274, 755
- Hivon, E., Guiderdoni, B., Bouchet, F., 1997, *in preparation*
- Hughes, D.H., Dunlop, J.S., Rawlings, S., 1997, astro-ph/9705094
- Kauffmann, G.A.M., 1995, MNRAS, 274, 161
- Kauffmann, G.A.M., 1996, MNRAS, 281, 487
- Kauffmann, G.A.M., White, S.D.M., 1993, MNRAS, 261, 921
- Kauffmann, G.A.M., White, S.D.M., Guiderdoni, B., 1993, MNRAS, 264, 201
- Kauffmann, G.A.M., Guiderdoni, B., White, S.D.M., 1994, MNRAS, 267, 981
- Kauffmann, G.A.M., Charlot, S., White, S.D.M., 1996, MNRAS, 283, L117
- Kennicutt, R.C., 1989, ApJ, 344, 685
- Kennicutt, R.C., 1997, in *Starbursts: Triggers, Nature and Evolution*, B. Guiderdoni and A. Kembhavi (eds.), Editions de Physique /Springer-Verlag
- Kennicutt, R.C., Tamblyn, P., Congdon, C.W., 1994, ApJ, 435, 22
- Lacey, C., Silk, J., 1991, ApJ, 381, 14
- Lacey, C., Guiderdoni, B., Rocca-Volmerange, B., Silk, J., 1993, ApJ, 402, 15
- Lanzetta, K.M., Wolfe, A.M., Turnshek, D.A., 1995, ApJ, 440, 435
- Lilly, S.J., Tresse, L., Hammer, F., Crampton, D., Le Fèvre, O., 1995, ApJ, 455, 108
- Lilly, S.J., Le Fèvre, O., Hammer, F., Crampton, D., 1996, ApJ, 460, L1
- Lonsdale, C.J., Hacking, P.B., Conrow, T.P., Rowan-Robinson, M., 1990, ApJ, 358, 60
- Lobo, C., Guiderdoni, B., 1997, *in preparation*
- Lonsdale, C.J. 1996, in *Unveiling the Cosmic Infrared Background*, E. Dwek (ed.), AIP Conference Proceedings 348

Loveday, J., Peterson, B.A., Efstathiou, G., & Maddox, S.J. 1992, *ApJ*, **390**, 79

Madau, P., Ferguson, H.C., Dickinson, M.E., Giavalisco, M., Steidel, C.C., Fruchter, A., 1996, *MNRAS*, **283**, 1388

Maffei, B. 1994, PhD Dissertation, Université Paris VII

Marzke, R.O., Huchra, J.P., Geller, M.J., 1994, *ApJ*, **428**, 43

Mathis, J.S., Mezger, P.G., Panagia, N., 1983, *A&A*, **128**, 212

McGaugh, S.S. 1994, *Nat.*, **367**, 538

Mushotzky, R.F., Loewenstein, M., 1997, *astro-ph/9702149*

Natarajan, P., Pettini, M., 1997, *astro-ph/9709014*

Natta, A., Panagia, N., 1984, *ApJ*, **287**, 228

Navarro, J.F., White, S.D.M., 1993, *MNRAS*, **265**, 271

Oliver, S.J., Rowan-Robinson, M., Saunders, W., 1992, *MNRAS*, **256**, 15P

Oliver, S.J., Goldschmidt, P., Franceschini, A., Serjeant, S.B.G., Efstathiou, A.N., *et al.*, 1997, *MNRAS*, **287**, 1

Pearson, C., Rowan-Robinson, M., 1996, *MNRAS*, **283**, 174

Pei, Y.C., Fall, S.M., 1995, *ApJ*, **454**, 69

Pettini, M., Steidel, C.S., Dickinson, M., Kellogg, M., Giavalisco, M., Adelberger, K.L., 1997, *astro-ph/9707200*

Puget, J.L., Abergel, A., Boulanger, F., Bernard, J.P., Burton, W.B., *et al.*, 1996, *A&A*, **308**, L5

Reach, W.T., *et al.* 1995, *astro-ph 9504056*

Rice, W., Lonsdale, C.J., Soifer, B.T., Neugebauer, G., Kopan, E.L., Lloyd, L.A., de Jong, T., Habing, H.J., 1988, *ApJSS*, **68**, 91

Rigopoulou, D., Lawrence, A., Rowan-Robinson, M., 1996, *MNRAS*, **278**, 1049

Rocca-Volmerange, B., Guiderdoni, B., 1988, *A&ASS*, **75**, 93

Rowan-Robinson, M., 1992, *MNRAS*, **258**, 787

Rowan-Robinson, M., Broadhurst, T., Lawrence, A., McMahon, R.G., Lonsdale, C., *et al.*, 1991a, *Nature*, **351**, 719

Rowan-Robinson, M., Saunders, W., Lawrence, A., Leech, K., 1991b, *MNRAS*, **253**, 485

Rush, B., Malkan, M., Spinoglio, L., 1993, *ApJS*, **89**, 1

Sanders, D.B., Mirabel, I.F., 1996, *ARAA*, **34**, 749

Saunders, W., Rowan-Robinson, M., Lawrence, A., Efstathiou, G., Kaiser, N., Ellis, R.S., Frenk, C.S., 1990, *MNRAS*, **242**, 318

Sawicki, M.J., Lin, H., Yee, H.K.C., 1997, *AJ*, **113**, 1

Schaeffer, R., Silk, J., 1985, *ApJ*, **292**, 319

Schaller, G., Schaerer, D., Meynet, G., Maeder, A., 1992, *A&ASS*, **96**, 269

Smith, B.J., Kleinmann, S.G., Huchra, J.P., Low, F.J., 1987, *ApJ*, **318**, 161

Soifer, B.T., Sanders, D.B., Madore, B.F., Neugebauer, G., Danielson, G.E., *et al.*, 1987, *ApJ*, **320**, 238

Soifer, B.T., Neugebauer, G., 1991, *AJ*, **101**, 354

Stark, A.A., Davidson, J.A., Harper, D.A., Pernic, R., Loewenstein, R., Platt, S., Engargiola, G., Casem, S., 1989, *ApJ*, **337**, 650

Steidel, C.C., Giavalisco, M., Pettini, M., Dickinson, M., Adelberger, K.L., 1996, *ApJ*, **462**, L17

Storrie-Lombardi, L.J., McMahon, R.G., Irwin, M.J., 1996, *MNRAS*, **283**, L79

Thornton, K., Gaudlitz, M., Janka, H.T., Steinmetz, M., 1997, *astro-ph/9706175*

Wang, B., 1991a, *ApJ*, **374**, 456

Wang, B., 1991b, *ApJ*, **374**, 465

White, S.D.M., Rees, M.J., 1978, *MNRAS*, **183**, 341

White, S.D.M., Frenk, C.S., 1991, *ApJ*, **379**, 52

Williams, R.E., *et al.*, 1996, *AJ*, **112**, 1335

Zurek, W.H., Quinn, P.J., Salmon, J.K., 1988, *ApJ*, **330**, 519

Zepf, S.E., Koo, D.C., 1989, *ApJ*, **337**, 34

APPENDIX A: MASS DISTRIBUTION OF COLLAPSED HALOES

The initial, linear perturbation is assumed to be spherical and homogeneous. This is the so-called “top-hat” model, which has the friendly property of being entirely defined by two parameters, for instance the size R and density contrast $(\delta\rho/\rho)_{z=0} \equiv \delta_0$ which are the linearly-extrapolated values at $z = 0$, or, equivalently, by the mass M and collapse redshift z_{coll} . If ρ_0 is the current mass density of the universe, we have $M = (4\pi/3)R^3\rho_0$.

The linearly-extrapolated density contrast, and the ratio of the radius of maximal expansion r_m to the linearly-extrapolated size R , can be respectively computed as functions of the redshift of collapse:

$$\delta_0 = \delta_0[1 + z_{coll}], \quad r_m/R = r_m/R[1 + z_{coll}]. \quad (A1)$$

For instance, if $\Omega_0 = 1$, $\delta_0 = \delta_c(1 + z_{coll})$ with $\delta_c = 1.68$, and $r_m/R = (3/5\delta_0)$. After collapse and violent relaxation, a mean potential forms and the virialized halo ends as a singular, isothermal sphere truncated at “virial radius” $r_V = r_m/2$. If we define a “circular velocity” as $V_c \equiv (GM/r_V)^{1/2}$, the density profile of the relaxed halo at $r \leq r_V$ is:

$$\rho_H(r) = \frac{V_c^2}{4\pi Gr^2}, \quad (A2)$$

and the mass included within radius r is simply $M(< r) = Mr/r_V$. For instance, if $\Omega_0 = 1$, the virial radius (in Mpc) and the circular velocity (in km s^{-1}) are:

$$r_V = 0.17 \left(\frac{M}{10^{12} M_\odot} \right)^{1/3} (1 + z_{coll})^{-1} h^{-2/3}, \quad (A3)$$

$$V_c = 160 \left(\frac{M}{10^{12} M_\odot} \right)^{1/3} (1 + z_{coll})^{1/2} h^{1/3}. \quad (A4)$$

We hereafter take $h \equiv H_0/(100 \text{ km s}^{-1} \text{ Mpc}^{-1})$. Finally, the virial temperature of the baryonic gas is:

$$T_V \equiv \frac{1}{2} \frac{\mu m_p}{k} V_c^2 = 35.9 \left(\frac{V_c}{\text{km s}^{-1}} \right)^2 K, \quad (A5)$$

m_p is the mass of the proton, and the mean molecular weight $\mu = 0.59$ corresponds to ionized gas with respective H and He mass fractions $X = 0.75$ and $Y = 0.25$.

Then we compute the mass distribution of collapsed haloes from the peaks formalism (Bardeen *et al.* 1986), as in Lacey and Silk (1991) and Lacey *et al.* (1993). We start from the power spectrum of linear fluctuations $P(k)$ which is normalized by σ_8 , the variance at a top-hat smoothing radius $R = 8h^{-1}$ Mpc. The peaks formalism uses momenta of the power spectrum with Gaussian smoothing on radius R_G . The mass included within such a radius is $M = (2\pi)^{3/2} R_G^3 \rho_0$. So the relation between the Gaussian radius R_G and the top-hat radius R including mass M is simply $R_G = 0.64R$. These momenta are computed from:

$$\sigma_m(R_G)^2 = \frac{1}{8\pi^3} \int k^{2m} P(k) |W_k(kR_G)|^2 4\pi k^2 dk, \quad (A6)$$

where $W_k(y) = \exp(-y)$ is the Fourier transform of the Gaussian filtering function:

$$W(x) = \frac{1}{(2\pi R_G^2)^{3/2}} \exp\left(-\frac{|x|^2}{2R_G^2}\right). \quad (A7)$$

The (comoving) number density distribution of peaks $\nu \equiv$

$\delta_{0G}/\sigma_0(R_G)$ in which δ_{0G} is smoothed on the Gaussian scale R_G is:

$$\frac{\partial n_{pk}(R_G)}{\partial \nu} d\nu = n_{pk}(R_G) P(\nu, R_G) d\nu, \quad (\text{A8})$$

with:

$$n_{pk}(R_G) = \frac{c_\infty}{4\pi^2 R_\star^3}, \quad (\text{A9})$$

$$P(\nu, R_G) = \frac{1}{c_\infty} \exp -\frac{\nu^2}{2} G(\gamma, \gamma\nu), \quad (\text{A10})$$

such as $\int P(\nu, R_G) d\nu = 1$. The functions R_\star and γ are computed as:

$$R_\star(R_G) \equiv \sqrt{3} \frac{\sigma_1(R_G)}{\sigma_2(R_G)}, \quad \gamma(R_G) \equiv \frac{\sigma_1^2(R_G)}{\sigma_0(R_G) \sigma_2(R_G)}. \quad (\text{A11})$$

The constant $c_\infty = 0.6397$ and an analytic fit of the function $G(\gamma, \omega)$ is given by equ. (4.4) and (4.5) of Bardeen *et al.* (1986). If $P(k) \propto k^n$, it is easy to check that $\gamma(R_G)$ does not depend on R_G and that $R_\star(R_G) \propto R_G$. For $\Omega_0 = 1$, $h = 0.5$, and the CDM power spectrum with $-3 \leq n \leq 1$, we have slow variations: $0.55 < \gamma(R_G) \leq 0.8$ and $1.05 \leq R_\star(R_G)/R_G \leq 1.5$ for $0.1 \leq R_G \leq 100$ Mpc.

At that stage, we do not have the number density distribution of peaks per bin of density contrast *and* radius. For that purpose, we have to introduce, as in Lacey & Silk (1991), a suggestion by Bond (1988) who interprets equ. (A9) as the total number density of peaks $n_{pk}(> R_G)$ at scale $> R_G$. By derivating equ. (A8), it is easy to get:

$$\frac{\partial^2 n_{pk}}{\partial R_G \partial \nu} dR_G d\nu = -\frac{3d \ln R_\star}{R_G d \ln R_G} n_{pk}(R_G) P(\nu, R_G) dR_G d\nu. \quad (\text{A12})$$

We neglect the slow variation of $\gamma(R_G)$ with R_G . This is the number density of *all* peaks. We now need to count the peaks over a certain threshold ν_{th} for collapse, and we get the formation rate of haloes:

$$\frac{\partial^2 n_{for}}{\partial R_G \partial \nu_{th}} dR_G d\nu_{th} = \frac{\partial}{\partial \nu_{th}} \left(\int_{\nu_{th}}^{\infty} \frac{\partial^2 n_{pk}}{\partial R_G \partial \nu} d\nu \right) dR_G d\nu_{th}. \quad (\text{A13})$$

After a change of variables, we get the halo formation rate, since $\nu_{th} \equiv \delta_{0G,th}[1 + z_{coll}]/\sigma_0(R_G)$:

$$\begin{aligned} \frac{\partial^2 n_{for}}{\partial \ln M \partial (1 + z_{coll})} &= -n_{pk}(> R_G) \frac{d \ln R_\star}{d \ln R_G} P(\nu_{th}, R_G) \\ &\times \frac{1}{\sigma_0(R_G)} \frac{d \delta_{0G,th}[1 + z_{coll}]}{d(1 + z_{coll})}. \end{aligned} \quad (\text{A14})$$

In order to link the Gaussian smoothing to the top-hat formalism, we take $R_G = 0.64R$ and $\delta_{0G,th} \equiv \delta_0 \sigma_0(R)/\sigma_0(R_G)$. The total number of collapsed peaks at redshift $(1 + z)$ is obtained by integrating equ. (A14) on all redshifts larger than $(1 + z)$.

The number density continuously increases with time, at all masses, and contrarily to what is found from the Press-Schechter formalism. The peaks formalism follows the collapse of *all* peaks, and counts high peaks as well as the broader, shallower peaks in which these high peaks are included. This so-called “cloud-in-cloud” problem results in a possible overestimate of the total number of galaxies. As a matter of fact, the total number density of peaks at the low-mass end of the mass function varies as M^{-2} , and the total mass density grows logarithmically with the lower mass cut-off. Anyhow, since other astrophysical phenomena will

act to “suppress” galaxy formation in low-mass haloes, we find that this slow divergence is not too serious a problem.

Finally, we do not explicitly include the merging of galaxies in merging haloes. In our crude modelling, new galaxies form at each generation of peak collapse. This model could be fitted to the description of “active” objects such as luminous galaxies seen in the IR. Such a simplifying assumption is very similar to that of Haehnelt and Rees (1993) who modelled QSO formation in each generation of halo formation. The issue of merging should be explicitly addressed by making Monte-Carlo realizations of the halo merging history tree and monitoring the merging of galaxies in merged haloes, for instance with the dynamical friction time scale (Kauffmann *et al* 1993; Cole *et al.* 1994; and following works). Such studies show that the galaxy merging rate is relatively low, and that the resulting mass and luminosity functions do not differ significantly from those computed with cruder assumptions. More precisely, galaxy merging seems to be sufficient to make the 10 % fraction of giant galaxies which are elliptical, but does not produce a significant change in the slope of the luminosity function at faint magnitudes. The implementation of the astrophysics hereafter described into this type of code is clearly one of the next steps of our programme. Nevertheless, it is worthwhile to note that only merging following the slow process of dynamical friction has been currently modelled. Two-body encounters and tidal interactions, which trigger starburst activity as it clearly appears from observational evidence, are not modelled yet in the current Monte-Carlo codes.